Elsevier Editorial System(tm) for Chemical Engineering Journal

Manuscript Draft

Manuscript Number: CEJ-D-18-06546R2

Title: Enhancement of Red Emission and Site Analysis in Eu2+ Doped New-Type Structure Ba3CaK(PO4)3 for Plant Growth White LEDs

Article Type: Research Paper

Keywords: Phosphor; Ba3CaK(PO4)3; Sites-dependent photoluminescence; Plant growth; White LEDs

Corresponding Author: Professor Chongfeng Guo, Ph.D

Corresponding Author's Institution: Northwest University

First Author: Jinmeng Xiang

Order of Authors: Jinmeng Xiang; Jiming Zheng; Ziwei Zhou; Hao Suo; Xiaoqi Zhao; Xianju Zhuo, Ph.D; Niumiao Zhang, Dr.; Maxim S Molokeev, Dr.; Chongfeng Guo, Ph.D

Abstract: A novel compound Ba3CaK(PO4)3 (BCKP) with new-type structure was synthesized and its structure was determined by X-ray diffraction Rietveld refinement, in which crystal structure consists of Ba1O9, Ba2O12, Ba3O9, CaO8 and KO10 polyhedra, that's five cationic sites. As a phosphor host, Eu2+ doped BCKP emits cold white light with about 90% quantum efficiency (QE) through entering different cationic sites. Based on the results of refinement, three Eu2+ luminescence centers in sites Ca, Ba2 and K were clearly assigned in Eu2+ solely doped BCKP by the time-resolved emission spectra (TRES), Van Uitert equation, but the emissions of Eu2+ at Ba1 and Ba3 sites are not easy to be determined for the same coordination number (CN). According to their different spatial distribution of the coordinated atoms, the first-principles calculation was used to compute the d orbital splitting energy of Eu2+ ions in Ba1 and Ba3 sites to accurately distinguish the ambiguous luminescence centers. In order to meet the requirement of plant growth spectra, Mn2+ was introduced into BCKP: Eu2+ to enhance the red component of spectra, which not only perfectly match with the absorption spectra of carotenoid and chlorophyll-b, but also LEDs fabricated through combining 365 nm near ultraviolet (n-UV) chip with BCKP: Eu2+, Mn2+ phosphor exhibit excellent parameters including high color rendering index (Ra) (92), excellent correlated color temperature (CCT) (4486 K) and outstanding QE up to 65%. Results confirmed that BCKP: Eu2+/Mn2+ phosphor with great potential applications in white LEDs and plant growth.

Response to Reviewers: Dear editor,
We are pleasure to accept your decision and the reviewers' suggestion. We would like to thank the referees for providing us constructive and valuable queries in bettering our manuscript in the revision. According to the remaining questions of referees, we have answered those questions raised by the referees carefully, and necessary changes have been made in the text. For the received queries, the replies are given below, and the changes in the manuscript have been marked in italic red color letters to show clearly.

Reviewers' comments:
Reviewer #1: The authors response well to the reviewers' comments and I therefore recommend its publication in Chem. Eng. J.
Answer to comments: Thanks for the reviewer's recognition of our answers.

Reviewer #3: Compared with the original version, a significant amount of work has gone into the revision of this paper, which has improved it considerably. In my opinion, it is acceptable for publication at its present form.
Answer to comments: Thanks for the reviewer's recognition of our answers.

Reviewer #9:
Question 1: The authors suggested that the results of BCKP structure refinement will convince readers in spite that Biso of cations were over 2 and those for oxygens were over 3. However, as a crystallographer, the suggested crystal structure was less than satisfactory. In addition, the authors discussed the emission properties of BCKP based on the insufficient structure.
Answer: About this question, we tried several models to decrease thermal parameters, including anisotropic preferred orientation, surface roughness intensity correction, Ba/Ca ratio refinement for all Ba sites, but only small change for thermal parameters with small decrease of R-factors (for example, from RBragg = 2.59% to 2.52% using Ba/Ca ratio refinement) were achieved. In parallel, we also asked the Rietveld community to give comment on these Biso parameters and all four scientists answered that all parameters values are normal and we should not expect high-quality values because CuKa patterns have very low reflection intensities at high-angle. Moreover, many structures with big thermal parameters for Ba ions (1.5-3.06 Å2) were published in high level journals (JACS, Chem. Comm., etc.), for example:
a) Biso(Ba) in the range of 2.06-2.43 Å2 published in Kazin, P.E., Zykin, M.A., Trusov, L.A., Eliseev, A.A., Magdysyuk, O.V., Dinnebier, R.E., Kremer, R.K., Felser, C. and Jansen, M., 2017. Chemical Communications, 53(39):5416-5419.
b) Biso(Ba) in the range of 1.55-3.06 Å2 published in Sedlmaier, S.J., Döblinger, M., Oeckler, O., Weber, J., Schmedt auf der Günne, J. and Schnick, W., 2011. Journal of the American Chemical Society, 133(31):12069-12078.
c) Biso(Ba) = 2.16 Å2 published in Lopes, A.M., Oliveira, G.N. and Ferdov, S., 2013. Solid State Sciences, 26:59-64.
d) Biso(Ba) = 1.8 Å2, Biso(Cu)= 3.08 Å2 published in Etheredge, K.M., Mackay, R., Schimek, G.L. and Hwu, S.J., 1996. Inorganic Chemistry, 35(26):7919-7921.
As for the Biso(O) one can found numerous examples with Biso even bigger 3-4, just for example:
e) Biso(O) in the range of 2.25-4.38 Å2 Ezzaafrani, M., Ennaciri, A., Harcharras, M. and Capitelli, F., 2014. 189(12):1841-1850.
f) Biso(O) = 2.08 Å2 Khan, M.A., Li, Y.Y., Lin, H., Zhang, L.J., Liu, P.F., Zhao, H.J., Duan, R.H., Wang, J.Q. and Chen, L., 2016. Syntheses of six and twelve membered borophosphate ring structure with nonlinear optical activity. Journal of Solid State Chemistry, 243: 259-266.

In our paper, these "big" values in our case can be associated with:
1) The structural defects (vacancies) in sites. For example, Ba and O sites both can contain vacancies. This model is very hard to refine, it is unstable due to big number of refined parameters. Especially it is hard to do using pattern measured with CuKa radiation.

2) The complex model of absorption prevents the correct refinement. Only transmission geometry (e.g. using capillary) allow using appropriate absorption model. In our case only Bragg-Brentano diffraction from surface was available.
3) Both of above
4) The Ba3 has the highest Biso and high coordination number 12, which can be owing to the bigger void and bigger oscillations.
5) Improper space group. We checked the possibility to low symmetry. However, all heavy ions and even P ion sit in special site on the "3" axis:

Site	X	Y	Z
Ba1	0	0	0
Ba2	0	0	0.753529(38)
Ba3	0	0	0.87621(15)
Ca	0	0	0.27033(17)
K	0	0	0.47333(17)
P1	0	0	0.16043(24)
P2	0	0	0.37557(49)
P3	0	0	0.58684(23)

(Only O ions sit in general sites)
and, therefore:
5.1) The lowering symmetry from R3m (current) to R3 will not lead to the splitting of (0,0,z) site and will not move ions to another position.
5.2) Lowering to P3 space group must lead to increasing 3 times of the number reflections (superstructure peaks). But we didn't see any superstructure peak.
5.3) Lowering to P1 space group should lead to peak broadening, but we didn't see it. All peaks are narrow.
5.4) All other cases are combinations of 5.1-5.3 cases.
So we think that R3m is very reasonable space group.
Thus, we think that the structural model in our manuscript is acceptable because bond lengths are correct; Checkcif and PLATON checking was successfully passed; symmetry was checked in PLATON also without any violations; low Rbragg factor = 2.59 % was obtained. As for the Biso, they are similar with those of published in other works and we didn’t use these values in any speculation or conclusions.

Question 2: The authors answered that site occupancy of Eu2+ in multi-sites host is random and the accurate amount of Eu2+ in each site is difficult to be determined despite that it was described in introduction that the site occupancy of Eu2+ in the BCKP host was investigated. These were inconsistent with each other. Which is correct?
Answer: Sorry for our unclear expression about the sites analysis. In this paper, an important aim is to figure out the relationship between the multiple cationic sites and luminescence centers in our work, which assigned the emission band to the special luminescent center at the corresponding cationic sites instead of the accurate amount of the dopant Eu2+. Here, we used the Sites-dependent PL Spectra to achieve our aims and shown in the part of Results and Discussion (3.2). Therefore the sites analysis or site-dependent spectra analysis are much closer to our work than that of site occupancy, necessary changes in the manuscript have been marked in italic red color letters to show clearly.

Question: The authors tried to assign each emission band to a crystallographic site replaced by Eu2+. Criterion of the assignment was coordination number and bond length to ligands. However, the authors have also done DOS calculation. Why were such indirect sluggish procedures

used? If you could calculate DOS and the contribution from d-orbital, you should estimate d-level splitting from the results.
Answer: Firstly, according to Van Uitert equation, the luminescence centers of Eu2+ in Ba2, Ca and K sites have been estimated easily because of their significant difference of the coordination number (CN) and ionic radius. However, with same CN and ionic radius, the relationship between Ba1/3 and remaining luminescence centers cannot be distinguished accurately. To address this question, electron structure of each situation should be compared in detail, and the first principle calculation giving real valence electrons structure was carried out in order to compare the crystal strength of Ba1 and Ba3 sites accurately. However, when change to the first principle point of view, the original picture used in luminescent analysis field (Fig. R1) is replaced by Bloch representation treating the electrons as waves travelling in the crystal lattice. Even for d or f electrons are inner valence electrons, they still can hop among atoms. Thus, computational results by first principle generally cannot give energy level diagram by continuous density of states (DOS), unfortunately, from which it is difficult to tell the difference between d orbitals directly. As shown in Fig. R3, the distribution of electron in different energy is diffuse, therefore we cannot obtain accurate energy level from DOS and also cannot directly compare the energy level splitting just like what is shown in Fig. R1. Fortunately, another energy level splitting, the splitting between binding and anti-binding states of Eu-O bonds, can help us (Fig. R2). The strength of crystal field shows positive correlation with the strength of Eu-O bonds, which can be expressed by Δc. Thus, we measured the splitting between binding and anti-binding states (Fig. R3) to compare the crystal field strength of Eu2+ in Ba1 and Ba3 sites.

Figure R1. The splitting of Eu 5d orbitals under crystal field.

Figure R2. The binding and anti-binding states of Eu-O bond.

Figure R3. The dz2-orbital splitting energy level of Eu2+ doped into Ba1 site.

We are again grateful to the reviewers for the valuable suggestions to improve the manuscript. Hopefully, our answers to those comments are acceptable to the editor.

Yours Sincerely
Prof. Chongfeng Guo

Cover Letter

Dear editor,

On behalf of all authors, I would like to submit our manuscript entitled "*Enhancement of Red Emission and Site Analysis in Eu^{2+} Doped New-Type Structure $Ba_3CaK(PO_4)_3$ for Plant Growth White LEDs*" for publication as an article in the ***Chemical Engineering Journal***.

Photosynthesis process is the basic for plant growth, whcih needs energy from the light. The pigments of chlorophyll a, b and bacteriochlorophyll are responsible for the absorption of light, in which blue and red light is direct promote the plant growth and enhancement of nurtiments. It is an efficient method to improve crop yields and quality and tune the growth cycle of plant through synergistic effect of blue and red light. It is important for plant to support absorbable light, and phosphhor-converted light emitting diodes (pc-LEDs) is a low-cost, energy-saving and enviromental friendly devices for plant growth. To develop a phosphor with emission covering the blue and red light is urgent. In here, a novel compound $Ba_3CaK(PO_4)_3$ (BCKP) with new-type structure was synthesized and its structure was determined by X-ray diffraction Rietveld refinement, in which crystal structure consists of $Ba1O_9$, $Ba2O_{12}$, $Ba3O_9$, CaO_8 and KO_{10} polyhedra, that's five cationic sites. As a phosphor host, Eu^{2+} doped BCKP emits cold white light with about 90% quantum efficiency (QE) through entering different cationic sites. Based on the results of refinement, three Eu^{2+} luminescence centers in sites Ca, Ba2 and K were clearly assigned in Eu^{2+} solely doped BCKP by the time-resolved emission spectra (TRES), Van Uitert equation, while the emissions of Eu^{2+} at Ba1 and Ba3 sites are further determined according to the calculated the *d* orbital splitting energy of Eu^{2+} ions in Ba1 and Ba3 sites by *first-principles calculation* to accurately distinguish the ambiguous luminescence centers. In order to meet the requirement of plant growth spectra, Mn^{2+} was introduced into BCKP: Eu^{2+} to enhance the red component of spectra, which not only perfectly match with the absorption spectra of carotenoid and chlorophyll-b, but also LEDs fabricated through combining 365 nm near ultraviolet (n-UV) chip with BCKP: Eu^{2+}, Mn^{2+} phosphor exhibit excellent parameters including high color rendering index (Ra=92), excellent correlated color temperature (CCT=4486 K) and outstanding QE up to 65%. Results confirmed that BCKP: Eu^{2+}/Mn^{2+} phosphor with great potential applications in white LEDs and plant growth.

This is why we chose your prestigious journal to present our results.

In the past two years, we have obtained some new results ***in this field*** and published in some famous journal, and all of the papers ***have been cited many times*** according to records of google scholar, which indicates that our research gain recognition of readers in related fields:

■ Ziwei Zhou, Jiming Zheng, Rui Shi, Niumiao Zhang, Jiayu Chen, Ruoyu Zhang, Hao Suo, Ewa M. Goldys and **Chongfeng Guo*** "*Ab Initio* Site Occupancy and Far-red Emission of Mn^{4+} in Cubic-phased $La(MgTi)_{1/2}O_3$ for Plant Cultivation" ***ACS Applied Materials & Interfaces 2017, 9（7）: 6177-6185 (Cited times 23)***

■ Hao Suo, Xiaoqi Zhao, Zhiyu Zhang, Ting Li, Ewa M. Goldys and **Chongfeng Guo*** "Constructing Multiform Morphologies of YF_3: Er^{3+}/Yb^{3+} Up-conversion Nano/Micro-crystals towards Sub-tissue Thermometry" ***Chemical Engineering Journal 2017, 313:65-73(Cited times 27, ESI 1%)***

■Jinmeng Xiang, Jiayu Chen, Niumiao Zhang, **Hebao Yao***, **Chongfeng Guo*** "Far Red and Near Infrared Double-Wavelength Emitting Phosphor Gd_2ZnTiO_6: Mn^{4+}, Yb^{3+} for Plant Cultivation LEDs" ***Dyes and Pigments 2018,154:257-262***

■Niumiao Zhang, Yi-Ting Tsai, Mu-Huai Fang, Chong-Geng Ma, Agata Lazarowska, Sebastian Mahlik, Marek Grinberg, Chang-Yang Chiang, Wuzong Zhou, Jauyn Grace Lin, Jyh-Fu Lee, Jiming Zheng, **Chongfeng Guo***, Ru-Shi Liu*,"Aluminate Red Phosphor in Light-Emitting Diodes: Theoretical Calculations, Charge Varieties and High-Pressure Luminescence Analysis" ***ACS Applied Materials & Interfaces 2017,9:23995-24004 (Cited times 2)***

■ Jiayu Chen, Niumiao Zhang, **Chongfeng Guo***, Fengjuan Pan, Xianju Zhou, Hao Suo, Xiaoqi Zhao, Ewa. M. Goldys "Site-dependent Luminescence and Thermal Stability of Eu^{2+} Doped Fluorophosphate towards White LEDs for Plant Growth" ***ACS Applied Materials & Interfaces 2016, 8(32):20856-20864 (Cited times 37)***

So we believe that this time you will take into account our efforts and will give us a chance to publish in your journal. I would like to assure that our results are uniquely exceptional and the readers will definitely benefit from the results of our investigations. In addition, the article is original and never been published previously, it is not under consideration for publication elsewhere. I hope that the referees will find our research results interesting and acceptable for publication in this journal.

Thank you in advance for your consideration.

With kind regards,

Sincerely yours

Professor Chongfeng Guo

E-mail: guocf@nwu.edu.cn ;

Fax & Tel.: 086-29-88302661

List of Suggested Reviewers

Professor Jing Wang:

School of Chemistry and Chemical Engineering, Sun Yat-Sen University

E-mail: ceswj@mail.sysu.edu.cn

Professor Zuoling Fu:

College of Physics, Jilin University

E-Mail: zlfu@jlu.edu.cn

Professor Hyun Kyoung Yang:

LED Convergence Engineering, Pukyong National University

E-mail:hkyang@pknu.ac.kr

Responses to the Second Comments

Dear editor,

We are pleasure to accept your decision and the reviewers' suggestion. We would like to thank the referees for providing us constructive and valuable queries in bettering our manuscript in the revision. According to the remaining questions of referees, we have answered those questions raised by the referees carefully, and necessary changes have been made in the text. For the received queries, the replies are given below, and the changes in the manuscript have been marked in *italic red color letters* to show clearly.

Reviewers' comments:

Reviewer #1: The authors response well to the reviewers' comments and I therefore recommend its publication in Chem. Eng. J.

Answer to comments: Thanks for the reviewer's recognition of our answers.

Reviewer #3: Compared with the original version, a significant amount of work has gone into the revision of this paper, which has improved it considerably. In my opinion, it is acceptable for publication at its present form.

Answer to comments: Thanks for the reviewer's recognition of our answers.

Reviewer #9:

Question 1: The authors suggested that the results of BCKP structure refinement will convince readers in spite that Biso of cations were over 2 and those for oxygens were over 3. However, as a crystallographer, the suggested crystal structure was less than satisfactory. In addition, the authors discussed the emission properties of BCKP based on the insufficient structure.

Answer: About this question, we tried several models to decrease thermal parameters, including anisotropic preferred orientation, surface roughness intensity correction, Ba/Ca ratio refinement for all Ba sites, but only small change for thermal parameters with small decrease of R-factors (for example, from RBragg = 2.59% to 2.52% using Ba/Ca ratio refinement) were achieved. In parallel, we also asked the Rietveld community to give comment on these Biso parameters and all four

scientists answered that all parameters values are normal and we should not expect high-quality values because CuKa patterns have very low reflection intensities at high-angle. Moreover, many structures with big thermal parameters for Ba ions (1.5-3.06 $Å^2$) were published in high level journals (JACS, Chem. Comm., *etc*.), for example:

a) Biso(Ba) in the range of 2.06-2.43 $Å^2$ published in Kazin, P.E., Zykin, M.A., Trusov, L.A., Eliseev, A.A., Magdysyuk, O.V., Dinnebier, R.E., Kremer, R.K., Felser, C. and Jansen, M., 2017. Chemical Communications, 53(39):5416-5419.

b) Biso(Ba) in the range of 1.55-3.06 $Å^2$ published in Sedlmaier, S.J., Döblinger, M., Oeckler, O., Weber, J., Schmedt auf der Günne, J. and Schnick, W., 2011. Journal of the American Chemical Society, 133(31):12069-12078.

c) Biso(Ba) = 2.16 $Å^2$ published in Lopes, A.M., Oliveira, G.N. and Ferdov, S., 2013. Solid State Sciences, 26:59-64.

d) Biso(Ba) = 1.8 $Å^2$, Biso(Cu)= 3.08 $Å^2$ published in Etheredge, K.M., Mackay, R., Schimek, G.L. and Hwu, S.J., 1996. Inorganic Chemistry, 35(26):7919-7921.

As for the Biso(O) one can found numerous examples with Biso even bigger 3-4, just for example:

e) Biso(O) in the range of 2.25-4.38 $Å^2$ Ezzaafrani, M., Ennaciri, A., Harcharras, M. and Capitelli, F., 2014. 189(12):1841-1850.

f) Biso(O) = 2.08 $Å^2$ Khan, M.A., Li, Y.Y., Lin, H., Zhang, L.J., Liu, P.F., Zhao, H.J., Duan, R.H., Wang, J.Q. and Chen, L., 2016. Syntheses of six and twelve membered borophosphate ring structure with nonlinear optical activity. Journal of Solid State Chemistry, 243: 259-266.

In our paper, these “big” values in our case can be associated with:

1) The structural defects (vacancies) in sites. For example, Ba and O sites both can contain vacancies. This model is very hard to refine, it is unstable due to big number of refined parameters. Especially it is hard to do using pattern measured with CuKa radiation.

2) The complex model of absorption prevents the correct refinement. Only transmission geometry (*e.g.* using capillary) allow using appropriate absorption model. In our case only Bragg-Brentano diffraction from surface was available.

3) Both of above

4) The Ba3 has the highest Biso and high coordination number 12, which can be owing to the

bigger void and bigger oscillations.

5) Improper space group. We checked the possibility to low symmetry. However, all heavy ions and even P ion sit in special site on the "3" axis:

Site	X	Y	Z
Ba1	0	0	0
Ba2	0	0	0.753529(38)
Ba3	0	0	0.87621(15)
Ca	0	0	0.27033(17)
K	0	0	0.47333(17)
P1	0	0	0.16043(24)
P2	0	0	0.37557(49)
P3	0	0	0.58684(23)

(Only O ions sit in general sites)

and, therefore:

5.1) The lowering symmetry from R3m (current) to R3 will not lead to the splitting of (0,0,z) site and will not move ions to another position.

5.2) Lowering to P3 space group must lead to increasing 3 times of the number reflections (superstructure peaks). But we didn't see any superstructure peak.

5.3) Lowering to P1 space group should lead to peak broadening, but we didn't see it. All peaks are narrow.

5.4) All other cases are combinations of 5.1-5.3 cases.

So we think that R3m is very reasonable space group.

Thus, we think that the structural model in our manuscript is acceptable because bond lengths are correct; Checkcif and PLATON checking was successfully passed; symmetry was checked in PLATON also without any violations; low Rbragg factor = 2.59 % was obtained. As for the Biso, they are similar with those of published in other works and we didn’t use these values in any speculation or conclusions.

Question 2: The authors answered that site occupancy of Eu^{2+} in multi-sites host is random and the accurate amount of Eu^{2+} in each site is difficult to be determined despite that it was described

in introduction that the site occupancy of Eu^{2+} in the BCKP host was investigated. These were inconsistent with each other. Which is correct?

Answer: Sorry for our unclear expression about the sites analysis. In this paper, an important aim is to figure out the relationship between the multiple cationic sites and luminescence centers in our work, which assigned the emission band to the special luminescent center at the corresponding cationic sites instead of the accurate amount of the dopant Eu^{2+}. Here, we used the Sites-dependent PL Spectra to achieve our aims and shown in the part of Results and Discussion **(3.2)**. Therefore the sites analysis or site-dependent spectra analysis are much closer to our work than that of site occupancy, necessary changes in the manuscript have been marked in italic red color letters to show clearly.

Question: The authors tried to assign each emission band to a crystallographic site replaced by Eu^{2+}. Criterion of the assignment was coordination number and bond length to ligands. However, the authors have also done DOS calculation. Why were such indirect sluggish procedures used? If you could calculate DOS and the contribution from d-orbital, you should estimate d-level splitting from the results.

Answer: Firstly, according to Van Uitert equation, the luminescence centers of Eu^{2+} in Ba2, Ca and K sites have been estimated easily because of their significant difference of the coordination number (CN) and ionic radius. However, with same CN and ionic radius, the relationship between Ba1/3 and remaining luminescence centers cannot be distinguished accurately. To address this question, electron structure of each situation should be compared in detail, and the first principle calculation giving real valence electrons structure was carried out in order to compare the crystal strength of Ba1 and Ba3 sites accurately.

However, when change to the first principle point of view, the original picture used in luminescent analysis field (**Fig. R1**) is replaced by Bloch representation treating the electrons as waves travelling in the crystal lattice. Even for *d* or *f* electrons are inner valence electrons, they still can hop among atoms. Thus, computational results by first principle generally cannot give energy level diagram by continuous density of states (DOS), unfortunately, from which it is difficult to tell the difference between d orbitals directly. As shown in **Fig. R3**, the distribution of electron in different energy is diffuse, therefore we cannot obtain accurate energy level from DOS

and also cannot directly compare the energy level splitting just like what is shown in **Fig. R1**. Fortunately, another energy level splitting, the splitting between binding and anti-binding states of Eu-O bonds, can help us (**Fig. R2**). The strength of crystal field shows positive correlation with the strength of Eu-O bonds, which can be expressed by **Δc**. Thus, we measured the splitting between binding and anti-binding states (**Fig. R3**) to compare the crystal field strength of Eu^{2+} in Ba1 and Ba3 sites.

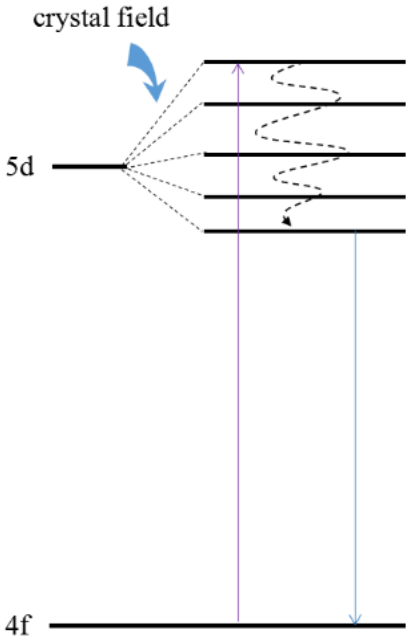

Figure R1. The splitting of Eu 5*d* orbitals under crystal field.

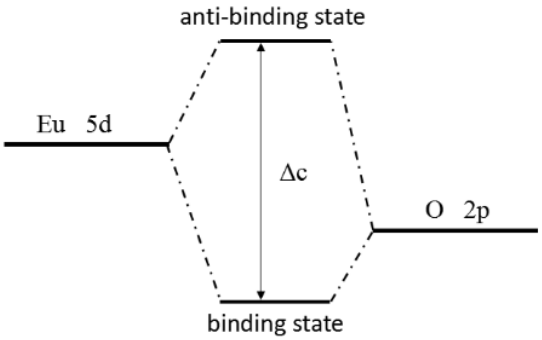

Figure R2. The binding and anti-binding states of Eu-O bond.

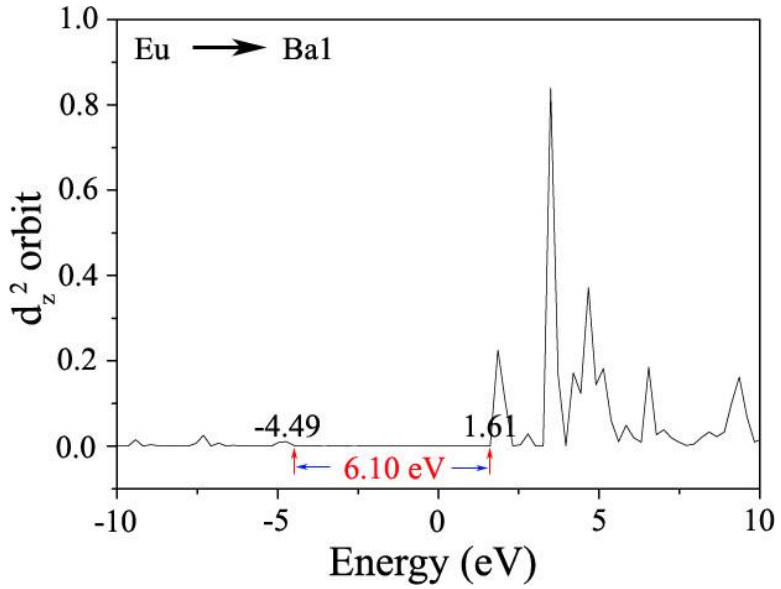

Figure R3. The d_z^2-orbital splitting energy level of Eu^{2+} doped into Ba1 site.

We are again grateful to the reviewers for the valuable suggestions to improve the manuscript. Hopefully, our answers to those comments are acceptable to the editor.

Yours Sincerely

Prof. Chongfeng Guo

Highlights

1. A novel compound $Ba_3CaK(PO_4)_3$ with new-type structure was developed.
2. Sites of Eu^{2+} in $Ba_3CaK(PO_4)_3$ were determined TRES, spectra and *calculation*
3. High efficient White light emission was obtained in BCKP: 1%Eu^{2+}.
4. Enhanced red emission in BCKP: Eu^{2+}/Mn^{2+} promote application in plant growth LED.

Enhancement of Red Emission and Site Analysis in Eu^{2+} Doped New-Type Structure $Ba_3CaK(PO_4)_3$ for Plant Growth White LEDs

Jinmeng Xiang[†], Jiming Zheng[†], Ziwei Zhou[†], Hao Suo[†], Xiaoqi Zhao[†], Xianju Zhou[#], Niumiao Zhang[†], Maxim S. Molokeev[‡, Δ, ⊥*] and Chongfeng Guo[†*]

[†] *National Key Laboratory of Photoelectric Technology and Functional Materials in Shaanxi Province, National Photoelectric Technology and Functional Materials & Application of Science and Technology International Cooperation Base, Institute of Photonics & Photon-Technology and Department of Physics, Northwest University, Xi'an 710069, China*

[#] *School of Science, Chongqing University of Posts and Telecommunications, Chongqing, 400065, P. R. China*

[‡] *Laboratory of Crystal Physics, Kirensky Institute of Physics, Federal Research Center KSC SB RAS, Krasnoyarsk 660036, Russia*

[Δ] *Siberian Federal University, Krasnoyarsk, 660041, Russia*

[⊥] *Department of Physics, Far Eastern State Transport University, Khabarovsk, 680021 Russia*

Corresponding authors

**E-mail: guocf@nwu.edu.cn (Prof. Guo)*

msmolokeev@mail.ru (Prof. Molokeev)

Abstract

A novel compound $Ba_3CaK(PO_4)_3$ (BCKP) with new-type structure was synthesized and its structure was determined by X-ray diffraction Rietveld refinement, in which crystal structure consists of $Ba1O_9$, $Ba2O_{12}$, $Ba3O_9$, CaO_8 and KO_{10} polyhedra, that's five cationic sites. As a phosphor host, Eu^{2+} doped BCKP emits cold white light with about 90% quantum efficiency (QE) through entering different cationic sites. Based on the results of refinement, three Eu^{2+} luminescence centers in sites Ca, Ba2 and K were clearly assigned in Eu^{2+} solely doped BCKP by the time-resolved emission spectra (TRES), Van Uitert equation, but the emissions of Eu^{2+} at Ba1 and Ba3 sites are not easy to be determined for the same coordination number (CN). According to their different spatial distribution of the coordinated atoms, the *first-principles calculation* was used to compute the *d* orbital splitting energy of Eu^{2+} ions in Ba1 and Ba3 sites to accurately distinguish the ambiguous luminescence centers. In order to meet the requirement of plant growth

spectra, Mn^{2+} was introduced into BCKP: Eu^{2+} to enhance the red component of spectra, which not only perfectly match with the absorption spectra of carotenoid and chlorophyll-b, but also LEDs fabricated through combining 365 nm near ultraviolet (n-UV) chip with BCKP: Eu^{2+}, Mn^{2+} phosphor exhibit excellent parameters including high color rendering index (Ra) (92), excellent correlated color temperature (CCT) (4486 K) and outstanding QE up to 65%. Results confirmed that BCKP: Eu^{2+}/Mn^{2+} phosphor with great potential applications in white LEDs and plant growth.

Keywords: Phosphor; $Ba_3CaK(PO_4)_3$; Sites-dependent photoluminescence; Plant growth; White LEDs

1. Introduction

Light not only affects the overall growth rhythm and development processes of plants, but also offers the energy source for plant cultivation. The artificial light supplement becomes necessary and popular for increasing production and quality or guiding the rhythm of plant in conventional indoor agriculture/horticulture and a short growing season or high latitude area with poor light [1, 2]. Red (600-700 nm) and blue (400-500 nm) light are dominant and responsible for phototropism and photosynthesis in the process of plant growth, respectively, which imply that it is more efficient for the artificial lighting with the capability of spectral composition control [3, 4]. Obviously, traditional artificial lighting sources cold-cathode fluorescent lamps (CCFLs) and gas discharge lamps (GDLs) suffer the serious mismatch between their emission spectra and the absorption of the main pigments chlorophylls and carotenoids in the process of photosynthesis [5]. Thus, light-emitting diodes (LEDs) used in modern agriculture as supplementary lighting source have been developed rapidly in recent decades due to their high light output with low radiant heat and controllable spectral composition [6]. Phosphor-converted light-emitting diodes (pc-LEDs) with mature fabrication technique are the most popular, in which several single-color emitting phosphors were excited by near-ultraviolet (n-UV) or blue LED chips and the true spectral composition control could be realized through adjusting the component of phosphors. In order to low the cost and enhance efficiency of pc-LEDs, it is necessary to avoid the re-absorption and different aging rate between each phosphor [7]. Single-phased multicolor-emitting phosphor is an ideal choice for dissolving above mentioned problems, and some phosphors with well-matched

double-emission band have been designed for plant growth LED based on energy transfer, such as Eu^{2+}, Mn^{2+} co-doped $A_3MgSi_2O_8$ (A = Ca, Sr, Ba) [8] and $Sr_2Mg_3P_4O_{15}$ [9] with strong blue and red emission. However, recent investigations illuminated that white light environment not only make operators worked in the green house comfortable [10], but also let plants grow better than those in blue plus red light environment on the premise of the matched emission wavelengths with photosynthetic active radiation [11].

For the *phosphors* used in plant growth lighting sources, the broad band emissions are perfect and well matched with the absorption spectra of plant growth pigments. Eu^{2+} doped *phosphors* usually *offer* a broad band emission due to its typical 4f-5d transitions and cold white light emission phosphor doped with Eu^{2+} have been developed in our group, in which site-dependent emission from the Eu^{2+} varied with the crystal field strength of the occupied cationic sites [12]. It is possible to search for a phosphor for plant growth LED through doping Eu^{2+} in a host with several cationic sites. Phosphate compounds with β-$Ca_3(PO_4)_2$-type structure are attractive phosphor hosts due to their versatile structural types and substation-induced tunable composition, in which there are five Ca^{2+} sites. Its formula could also be written as β-$Ca_{3n}(PO_4)_{2n}$ (n=1, 2, 3…) and Ca^{2+} can be partially substituted to construct more new phases with β-$Ca_3(PO_4)_2$-type, such as two univalent metal M^+ ions substitute one Ca^{2+} ion, two trivalent metal ions R^{3+} substitute three Ca^{2+} ions or one divalent metals ions substitute one Ca^{2+} ion, leading to a large number of new compounds $A_3(PO_4)_2$ (A = Ca, Sr, Ba) [13], $A_{10}M(PO_4)_7$ (A = Ca, Sr, Ba; M = Li, Na, K) [14] and $A_9R(PO_4)_7$ (A = Ca, Sr, Ba; R = Cr and rare earth) [15]. For Eu^{2+} doped phosphor with β-$Ca_3(PO_4)_2$-type structure, its emission spectrum could be effectively tuned through entering different sites because Eu^{2+} ions with f-d transition suffer different crystal field. The compound under investigation, $Ba_3CaK(PO_4)_3$ was achieved through six Ba^{2+} and two K^+ replace of six Ca^{2+} and one Ca^{2+} in β-$Ca_9(PO_4)_6$, respectively, to form the compound $Ba_6Ca_2K_2(PO_4)_6$, namely $Ba_3CaK(PO_4)_3$. However, the present cation replacement absolutely led to a new crystal structure, which was not determined yet and has never been discussed.

Here, the detailed structure of host material $Ba_3CaK(PO_4)_3$ (BCKP) was determined in real space by Monte-Carlo method with simulated annealing procedure and after that refined by Rietveld method, and the *site-dependent spectra analysis* of Eu^{2+} in the BCKP host was also investigated through photoluminescence at liquid helium temperature (LHT), time-resolved

emission spectra (TRES) and *first-principle calculation*. Eu^{2+} solely-doped sample displayed a cold white emission with outstanding QE (90%) under the near ultraviolet (n-UV) light excitation, Mn^{2+} ions were introduced to enhance the red spectral components through efficient energy transfer from Eu^{2+} to Mn^{2+} ions in order to match well with the absorption spectra of carotenoid and chlorophyll-b. The white LED devices with excellent Ra (92), CCT (4486 K) and QE (65%) have been fabricated by combining the 365 nm chip with the Eu^{2+}-Mn^{2+} co-doped BCKP, which is not only can be used for plant growth white LEDs, but also can make operators worked in indoor agriculture comfortable.

2. Material and methods

2.1. Synthesis and characterization.

A series of Eu^{2+} singly and Eu^{2+}-Mn^{2+} co-doped $Ba_3CaK(PO_4)_3$ (BCKP) were prepared *via* convenient high-temperature solid-state reaction method, in which analytical reagent (A. R.) $CaCO_3$, $BaCO_3$, K_2CO_3, $NH_4H_2PO_4$, $MnCO_3$ and high purity Eu_2O_3 (99.99%) were used as starting materials. The stoichiometric amount of raw materials was mixed thoroughly with appropriate volume ethanol in an agate mortar and then dried at 70℃ for 1 h. After that the dried the mixture was pre-sintered at 600 ^oC for 3 h, next to further calcine at 1250 ^oC for 8 h in CO reducing atmosphere to obtain the final products.

The structure and purity of samples were determined by powder X-ray diffraction (XRD), and the diffraction data of host material BCKP and BCKP: 1%Eu^{2+}, 20%Mn^{2+} for structural solving and Rietveld analysis were collected with a Bruker D8 ADVANCE powder diffractometer (Cu-$K\alpha$ radiation) and linear VANTEC detector at room temperature. The step size of 2θ was set as 0.016°, and the counting time was 10 and 15 s per step for BCKP and BCKP: 1%Eu^{2+}, 20%Mn^{2+}, respectively. The 2θ in range of 7-70º was measured with 0.6 mm divergence slit, but 2θ ranging 70-150º was measured with 2 mm divergence slit. Larger slits allow noticeable increase of intensity in high-angle peaks without loss of resolution because the high-angle peaks were broad enough to be not affected by bigger divergence beam. The esd's $\sigma(I_i)$ of all points on patterns were calculated using intensities I_i: $\sigma(I_i) = I_i^{1/2}$. The intensities and obtained esd's were further normalized: $I_{i\ norm} = I_i \times 0.6/(\text{slit width})$, $\sigma_{norm}(I_i) = \sigma(I_i) \times 0.6/(\text{slit width})$, taking into

account actual value of divergence slit width used to measure each particular intensity I_i and saved in xye-type file. So transformed powder pattern usually had view in whole 2θ range 5-140°, all high-angle points had small esd's. The crystal structure refinement was performed by using TOPAS 4.2 [16], in which each point of esd's was accounted by special weight scheme.

The photoluminescence emission (PL) and excitation (PLE) spectra at liquid helium temperature (LHT), temperature-dependent spectra, time-resolved emission spectra (TRES) as well as PL decay curves were measured on an Edinburgh FLS920 spectrophotometer equipped with a 450 W Xe lamp as the excitation source for the steady state spectra and an EPL-375 pulse laser as the pumping source for decay curves. An Oxford OptistatDN2 nitrogen cryogenics and CTI-Cryogenics temperature controlling system (with about 20 min duration time at the fixed temperature) were attached with FLS920 spectrometer to measure the temperature-dependent luminescent properties. The quantum efficiency (QE) was tested on the Quantaurus QY (C9920-02G, Japan) spectrometer.

2.2. Computation.

The *first-principle calculations* were performed within the framework of density functional theory (DFT), which was implemented in the *Vienna ab initio simulation package* (VASP). The exchange correlation was carried out using the generalized gradient approximation (GGA) *Perdew-Burke-Ernzerhof* (PBE) and the projector augmented wave (PAW) method potentials [17]. The plane-wave cutoff energy was set below 500 eV and the Brillouin zone was sampled with *Γ*-centered k-meshes of 12 × 12 × 2 on the basis of the Monkhorst and Pack (MP) method [18]. The optimized structures were established by *ab-initio computation*, in which the total energy convergence threshold of the unit cell was less than 10^{-5} eV/atom and the residual atomic forces was smaller than 10^{-3} eV/Å. A 2 ×2 × 1 supercell with 240 atoms was constructed using the structure of BCKP with *R3m* space group, in which twelve Ba1 and Ba3 were coordinated by nine oxygen atoms but their spatial distribution is different. Then single Ba1 or Ba3 was substituted by a Eu atom and the density of state (DOS) was calculated to analyze the luminescent properties according to their crystal environment and *d* orbital splitting. The detailed discussion would be given in the following part.

3. Results and discussion

3.1. XRD refinement of samples.

All peaks of $Ba_3CaK(PO_4)_3$ (BCKP) pattern were indexed by trigonal *R*-centered unit cell with parameters a = 5.4784 Å, c = 34.9043 Å, V = 907.24 $Å^3$ (GOF = 111.22). The most probable space groups are *R*3, *R*-3, *R*3*m*, *R*32 and *R*-3*m*. The structure solving in the lowest space groups, *R*3 will account for all possible solutions in higher space groups, therefore, it was initially decided to solve the structure in the *R*3 space group. The program TOPAS 4.2 [16] was used to solve the crystal structure. The charge flipping procedure and Patterson synthesize were used to localize heavy ions. It was clearly found that all big maximums of electron density are located in the *c*-axis. Taking into account the average volume of non-hydrogen ion is 17 $Å^3$, it was calculated that asymmetric unit cell contains $V/(17Å^3 \times Z)$ = 907.24 Å/(17 Å × 3) ≈ 18 ions. Formula $Ba_3CaK(PO_4)_3$ gives 20 ions and it was decided that three Ba^{2+}, one Ca^{2+}, one K^+ and three PO_4^{3-} ions are located in the *c*-axis. The structure was solved using a simulated annealing procedure to the randomized *z*-coordinates of two Ba^{2+} ions, one Ca^{2+}, one K^+ and three P^{5+} ions, the *x*, *y* coordinates of these ions were equal to 0 during solving. Moreover third Ba^{2+} ion was placed in (0, 0, 0) site and it was *z*-coordinated ion. So, it was totally used only 8 parameters. The dynamical occupancy correction of the atoms wasn't used. After the calculations, a solution was found with R_{wp} = 9.8%, R_B = 9.3%. Then, the Rietveld refinement was performed and the difference electron density based of F_{obs}-F_{calc} difference of the structural amplitudes revealed all O^{2-} ions near P^{5+} ions so that three PO_4 tetrahedra were formed. The structural analysis of $Ba_3CaK(PO_4)_3$ using the program PLATON [19] revealed additional element of symmetry, *m* plane, and the space group was changed to *R*3*m*. all O^{2-} ions were placed in the closest special sites and new cycle of refinement was performed. The R-factors rapidly dropped down R_{wp} = 6.63% and R_B = 6.04%. The final Rietveld refinement accounts spherical harmonic 2 order of preferred orientation, surface roughness. Isotropic thermal parameters of all ions were refined independently besides O^{2-} ions, which have only one thermal parameter in order to reduce number of refined parameters. Refinement was stable and gives low *R*-factors (Table 1, Figure 1a). Coordinates of atoms and main bond lengths are in Table S1 and Table S2, respectively.

Crystal structure $Ba_{2.97}Eu_{0.03}Ca_{0.8}Mn_{0.2}K(PO_4)_3$ was refined using model of $Ba_3CaK(PO_4)_3$,

all Ba sites were doped by Eu^{2+} ions and Ca sited was doped by Mn^{2+} according to suggested chemical formula. The concentration values were not refined due to low Eu^{2+} concentration and due to similarity of Ca and Mn atomic scattering functions. Refinement was also stable and gives low *R*-factors (Table 1, Figure 1b). Coordinates of atoms and main bond lengths are in Table 1S and Table 2S, respectively. It was found that cell volume of $Ba_{2.97}Eu_{0.03}Ca_{0.8}Mn_{0.2}K(PO_4)_3$ V = 908.48(1) Å3 is smaller than V = 909.74(3) $Å^3$ of $Ba_3CaK(PO_4)_3$ which is consistent with smaller ion radii (IR) of Mn IR(Mn^{2+}, CN = 8) = 0.96 Å in comparison with IR(Ca^{2+}, CN = 8) = 1.12 Å, and with smaller ion radii of Eu IR(Eu^{2+}, CN = 9) = 1.3 Å in comparison with IR(Ba^{2+}, CN = 9) = 1.47 Å [20]. All XRD patterns of the prepared samples are similar and depicted in Figure S1, which further confirm that Eu^{2+} and Mn^{2+} enter into the host successfully.

Cell parameter search in the ICSD database (Version 2018-1) didn't reveal any isostructural or similar compounds to $Ba_3CaK(PO_4)_3$. Compound with similar chemical formula $Pb_3CaNa(PO_4)_3$ (lacunary apatite) [21] has *P*63/*m* space group, another cell parameters and of course absolutely another crystal structure. Crystal structure $Ba_3CaK(PO_4)_3$ (Figure 1c) consists of BaO_9, BaO_{12}, CaO_8, KO_{10} polyhedra connected by vertexes, edges and faces forming 3D net, the tetrahedra voids between large polyhedra are filled by PO_4 tetrahedra. It is interesting that all polyhedra lie on the 3-fold axis and have high local symmetry with point symbol 3*m*, and this is noticeable different with structures $Ca_9MMn(PO_4)_7$ (M = Li, Na, K) (*R*3*c*) [22], $Na_2CaMg_7(PO_4)_7$ (chladniite) [23]. Crystal structure $Ba_2CaNa_3(PO_4)_3$ (*P*31*c*) [24], which can be obtained from $Ba_3CaK(PO_4)_3$ by changing $Ba^{2+} \rightarrow 2Na^+$, has $(Ca/Na)O_6$, BaO_9, BaO_{12} polyhedra on the 3-fold axis, but their local symmetry are only 3. It should be noted that in spite of crystal structures of $Ba_2CaNa_3(PO_4)_3$ and $Ba_3CaK(PO_4)_3$ are different and *c* cell parameters are also different, they have similar cell parameters a = 5.4515(2) and a = 5.48501(8) Å, respectively. Crystal structure $BaMgNa_2(PO_4)_2$ [25, 26] has only one Ba site with local symmetry -3 [25] or -3*m* [26] and this compound is centrosymmetric, but compound under consideration $Ba_3CaK(PO_4)_3$ is polar. Compound $Gd_2CaCs(PO_4)_3$ ($P6_322$) [27], which can be obtained from $Ba_3CaK(PO_4)_3$ by changing $3Ba^{2+} \rightarrow 2Gd^{3+}$ and $K^+ \rightarrow Cs^+$, consists of CsO_8 and $(Gd, Ca)O_8$ square antiprisms with local symmetry 222. So, compound $Ba_3CaK(PO_4)_3$ is new polar compound with unique set of Ba-Ca-K polyhedra possessing the highest local structure 3*m* among all polar trigonal compounds.

3.2. Sites-dependent PL spectra.

According to above crystal structure results, Eu^{2+} *ions* have chance to enter five different cationic sites in BCKP host, which make it reasonable to have five emission bands for BCKP: Eu^{2+} due to its crystal field strength dependent emission. Figure 2a displays the PL and PLE spectra of BCKP: 1%Eu^{2+} at room temperature, in which a broad and strong excitation band monitoring at 460 nm was observed in the range of 250 to 440 nm and the PLE spectrum matches well with the commercial n-UV LED chip. The present sample shows bright cold white light emission with an unsymmetrical band ranging from 400 to 675 nm under the excitation of 365 nm light, which hints that there are more than one luminescence centers in BCKP: 1%Eu^{2+} and its QE is about 90%. As mentioned above, Eu^{2+} ions can enter five cationic sites, in which different crystal field environments lead to the diverse emission wavelengths and lifetimes for Eu^{2+} ions.

To further prove the existence of multiple sites of Eu^{2+} and determine the number of luminescence centers, the normalized time-resolved emission spectra (TERS) of sample BCKP: 1%Eu^{2+} were measured at room temperature with the excitation of 375 nm EPL pulse laser, as shown in Figure 2b and c. A significant red-shift was observed in the two-dimensional TRES (in Figure 2b), implying the existence of multiple luminescence centers. No obvious shift was observed in the emission peak at the decay time ranging from 0 to 1 μs and 3 to 4.5 μs; whereas the maximum emission peak rapidly shift from 460 to 520 nm with decay time growing from 1.0 to 3.0 μs. Four representative normalized TRES at specific time 1.0, 1.5, 2.5 and 4.5 μs were used to confirm the accurate number of those luminescent centers, as shown in Figure 2c. Peak *b* in TRES was first detected at 1 μs; then peaks *c* and *d* gradually appeared with prolonging the time from 1 to 2.5 μs and the peaks *a* and *e* become clear with delaying the time to 4.5 μs. This result indicated the existence of five luminescence centers, which is contributed to five cationic sites occupied by activator Eu^{2+} ions.

The precise assignment of luminescent center emission position is difficult to identify at room temperature because of thermal vibration, thus the PL spectrum of Eu^{2+} doped BCKP at liquid helium temperature (LHT) was displayed in Figure 3 under the 365 nm n-UV light excitation. An asymmetric broad emission band ranging from 400 to 700 nm was observed in the PL spectrum, which could attribute to the typical emission of Eu^{2+} 5d → 4f transitions from different sites. The PL spectrum at LHT could be well fitted by the sum of five Gaussian peaks, bands centered at 443, 460, 481, 500 and 535 nm, respectively. Insets of Figure 3 give the

polyhedron of each cationic site. In order to assign the relationship between the luminescence centers and cationic sites, the Van Uitert equation is used to approximate estimate emission position of Eu^{2+} at five different cites: [28, 29]

$$E = Q\left[1-\left(\frac{V}{4}\right)^{\frac{1}{V}}\times 10^{-\frac{nEar}{80}}\right] \quad (1)$$

Here, E represents the energy position of the lower d-band edge for Eu^{2+} (cm^{-1}); Q (3400 cm^{-1} for Eu^{2+}) stands for the energy position for the low d-band edge of the free ion; V equals the valence of the cation (V = 2 for Eu^{2+}); n is the coordination number (CN) of the site occupied by activator ion; Ea is a constant in the same host; r is the radius of the cationic ion replaced by the activator. According to the CN of each cationic site, the radius of the five cationic sites decreased in the order of Ba2 (CN = 12, r = 1.61 Å) > K (CN = 10, r = 1.59 Å) > Ba1/Ba3 (CN = 9, r = 1.47 Å) > Ca (CN = 8, r = 1.12 Å). The Gaussian emission band peaked at 443, 500 and 535 nm was attributed to the emission of Eu^{2+} occupied the Ca, K and Ba2 sites, but it is impossible to distinguish the attribution of band centered at 460 and 481 from site Ba1 or Ba3 due to their same CN and radius. Fortunately, the crystal field strength is not only determined by the positive ionic radius and CN, but also by the type of the polyhedron and the bond length, *etc.* [30, 31]. Generally, the loose site means lower crystal field strength, which leads to smaller degree of crystal field splitting and higher-energy emission peak [32, 33]. For comparing the splitting degree strength of Eu^{2+} 5d orbits in sites Ba1 and Ba3, the bond length of Eu/Ba-O in two sites are listed in Table S1. Eu1(enter the sites of Ba1) is coordinated by 9 oxygen atoms with the average bond length 2.8236 Å, which is shorter than that of Eu3-O (2.8520 Å, at Ba3 site). Hence, the higher energy emission peak at 460 nm is probably originated from the 5d → 4f transitions of Eu^{2+} in Ba3 site, while the relative lower energy emission peak at 481 nm is ascribed to Eu^{2+} in Ba1 site.

3.3. Analysis of crystal field at Ba1 and Ba3.

In order to further identify the attribution of emission bands centered at 460 and 481 nm, the splitting of Eu^{2+} 5d orbits was determined through *first-principles computations*. First, the optimized structures of Eu^{2+} enter the Ba1 or Ba3 sites were established on the basis of the pristine BCKP structure, as shown in Figure 4a and b. It is found that the bond lengths of Eu1/3-O and Ba1/3-O in the optimized structure (in Table S3) is close to that of Rietveld refinement results,

which illuminates that the present optimized structures are reasonable. Based on this result, the PDOS on the *d* orbitals of Eu atom in Ba1 or Ba3 site were calculated using the *first-principles computations* (in Figure 4c and d), respectively.

As shown in the Figure 4c and d, the five PDOS spectra can be grouped into three groups in crystal field environment, including d_z^2, *degenerate* d_{xz} *and* d_{yz}, *and the other degenerate* d_{xy} *and* d_x^2-$_y^2$ *orbitals. And each PDOS spectrum has split into two parts: one above the* E_F *and the other below it, which is the splitting between binding and anti-binding states of Eu-O bonds. d-orbital splitting is attributed to the spherical symmetry breaking under purterbation of surrounding O atoms, and the stronger purterbation corresponds to the larger splitting. Here the strength of purterbation shows positive correlation with the strength of Eu-O bonds, and the latter is related to the splitting between binding and anti-binding states of Eu-O bonds [34].*

Comparing the splitting between binding and anti-binding states of the Eu1-O (in Ba1 site) and Eu3-O (in Ba3 site) bonds in different orbital groups, the splitting energy of Eu1 is obviously bigger (6.10 eV in d_z^2 *orbital*, 5.17 eV in d_{xz} and d_{yz} degenerate *orbitals*) than those of Eu3 (5.16 eV in d_z^2 *orbital*, 3.68 eV in d_{xz} and d_{yz} degenerate *orbitals*). These big differences derive from the shorter Eu1-O bond length than that of Eu3-O in vertical direction. *And* there are three O atoms around Eu1 but no O atoms around Eu3 in horizontal direction, which leads relatively weak interaction between degenerate *orbitals* d_x^2-$_y^2$, d_{xy} and surrounding O atoms for Eu3, thus the splitting energy of Eu^{2+} in degenerate *orbitals* d_x^2-$_y^2$ and d_{xy} is smaller for Eu3 (5.00 eV) in comparison with that of Eu1 (5.17 eV) in the PDOS spectra. *Based on above mentioned, the splitting degree of* Eu^{2+} *5d orbitals in Ba1 site is larger than that of* Eu^{2+} *5d levels in Ba3 site, implying a stronger crystal field for Eu in Ba1 site.* Therefore, the emission bands centered at 460 nm and 481 nm are attributed to the emission of Eu^{2+} in the sites of Ba3 and Ba1, respectively.

Above results accurately confirm that there are five Eu^{2+} luminescence centers, and the corresponding emission band centered at 443, 460, 481, 500 and 535 nm are from the Eu^{2+} occupied the sites of Ca, Ba3, Ba1, K and Ba2 in the host BCKP.

3.4. Thermal stability.

During the practical application of phosphor in LEDs, the working temperature of the LED chip would arrive at about 100 ℃. A perfect phosphor for LEDs should offer excellent thermal stability, which will be conductive to maintain high efficiency and long lifetime of the LEDs. As a result,

the temperature-dependent PL spectra of BCKP: 1%Eu^{2+} were showed in Figure 5a, in which the integrated intensity of sample continuously decreases with the temperature increase and remains at about 62% intensity at room temperature as heating up to 100 ^{o}C (Figure 5b). Generally, the emission intensity thermal quenching is attributed to non-radiative relaxation. With the temperature rising, more and more excited electrons absorb additional vibration energy to jump and arrive the cross point of ground and excited state, then the electrons return to the ground state in the form of releasing heat rather than light (inset of Figure 5b). The thermal quenching activation energy (E_a) can be figured out by the following formula: [35]

$$I_T = \frac{I_0}{1 + c\exp\left(-Ea/\kappa T\right)} \qquad (2)$$

Where I_T and I_0 represent emission intensities at experimental and room temperature, respectively; κ stands for the Boltzmann constant (κ = 8.617 × 10^{-5} eV/K); c (constant) is the rate of thermally activated escape. According to equation (2), the activated energy was calculated as E_a = 0.26 eV based on the slope of the straight line yielded by the plot of ln(I_0/I-1) *vs* 10000/T.

3.5. Enhancement of red component in Eu^{2+} doped BCKP.

The optimal composition of Eu^{2+} doped BCKP was determined according to the integrated intensities of PL spectra as function of Eu^{2+} concentration. As depicted in Figure S2, the intensity of samples first monotonously increase and arrive the maximum at 1% content. After that, the PL intensity rapidly decreases as the concentration of Eu^{2+} beyond 1% due to the concentration quenching effect, which is attributed to the non-radiative energy migration among the identical activator Eu^{2+} ions. From the PL spectra with different Eu^{2+} contents, it is found that the red component is deficient. However, the red light not only plays a super important role in photosynthetic apparatus development but also accelerates the accumulation of starch by inhabiting the translation of photosynthesis out of leaves [36, 37]; simultaneously, the red component is also benefit to obtain an ideal lighting source with improving CRI and CCT. Thus, it is necessary to enhance the weak red emission intensity for single-doped BCKP: Eu^{2+} in order to well meet the requirement of photosynthesis. It is an obvious approach through introduction Mn^{2+} in BCKP host because Mn^{2+} will has a orange to red emission in strong crystal field as it enters the sites of Ca in present new compound BCKP, in which efficient energy transfer (ET) from Eu^{2+} to Mn^{2+} is necessary. The PLE and PL spectra of Eu^{2+} and Mn^{2+} solely doped BCKP is showed in

Figure 6a and b, in which a significant spectral overlap was found between the PL spectrum of Eu^{2+}- and the PLE spectrum of Mn^{2+}-doped samples and the resonance-type energy transfer from Eu^{2+} to Mn^{2+} is possible occurred. After co-doping the Eu^{2+} and Mn^{2+} into the BCKP, the red component was greatly improved *(Figure S3)* and the PLE spectra of Eu^{2+} and Mn^{2+} co-doped BCKP phosphor are the similar under monitoring at 460 and 590 nm (Figure 6c), which further imply that the resonance-type energy transfer from Eu^{2+} to Mn^{2+} is existed. The decay curves of BCKP: 1%Eu^{2+}, *y*%Mn^{2+} were measured under the excitation of 375 nm and depicted in Figure 6d as a function of Mn^{2+} contents (*y*) to further confirm the occurrence of ET in the co-doped samples.

It is observed that the lifetime of Eu^{2+} gradually decline with the growth of Mn^{2+} concentration, and the decay curves can be well fitted with the second-order exponential decay model, as following equation: [38, 39]

$$I_t = I_0 + A_1 \exp\left(-\frac{t}{\tau_1}\right) + A_2 \exp\left(-\frac{t}{\tau_2}\right) \tag{3}$$

Here, I_0 and I_t are the luminescence intensity when times are 0 and *t*, respectively; A_1 and A_2 are fitting constants; τ_1 and τ_2 represent the fast and slow lifetimes for the exponential segment, respectively. According to the fitting results, the average lifetimes of Eu^{2+} monitored at 460 nm are calculated to be 501.79, 453.70, 412.27, 350.53, 273.64 ns with concentration of Mn^{2+} at y = 0, 5, 10, 15, 20, respectively. As the concentration of Mn^{2+} increasing, the average lifetimes decrease visibly, which further confirm the existence of ET from Eu^{2+} to Mn^{2+}. And the ET efficiency (η_τ) can be calculated by the equation: [40]

$$\eta_\tau = 1 - \frac{\tau}{\tau_0} \tag{4}$$

Where τ_0 and τ stand for the decay lifetimes of the sensitizer in singly and co-doped samples. The dependence of τ and η_τ on the Mn^{2+} concentration is displayed in inset of Figure 5b, where the ET efficiency rise from 0 to 45.5% with the contents of the Mn^{2+} increasing from 0 to 20%. And the ET process can be described as: the electrons of Eu^{2+} are pumped to excited state 5d from ground state 4f with the excitation of 365 nm n-UV light, and then non-radiatively (NR) back to the lowest excited level. Afterwards part of them back to the ground state with a cyan emission while the other part of energy transfer to Mn^{2+} resulting in the excitation of the electrons from ground

state to excited state, leading to the enhanced red emission by the ET process from Eu^{2+} to Mn^{2+} ions. *Meanwhile, the ET mechanism has also been investigated on the base of the Dexter's ET expression of exchange interaction and multi-polar interaction by the following relation: [41, 42]*

$$\frac{\eta_0}{\eta} \propto C^{\frac{\theta}{3}}, \quad \frac{I_0}{I} \propto C^{\frac{\theta}{3}} \tag{5}$$

Here, η_0 and η represent the luminescence quantum efficiency of Eu^{2+} ions with or without Mn^{2+} ions; C stands for the dope contents of Mn^{2+}; the value of η_0/η can be approximately estimated by the ratio of related luminescence intensities (I_0/I); θ = 3, 6, 8, and 10 corresponded to exchange interaction, dipole-dipole, dipole-quadrupole and quadrupole-quadrupole interaction, respectively. The most reasonable linear relation was observed when θ = 6 in the I_0/I vs $C^{\theta/3}$ plots, which imply the dipole-dipole mechanism dominates the $ET_{Eu\text{-}Mn}$ in the BCKP host (Figure S4).

3.6. Fabrication and performance of the white LED.

To evaluate the practical application of the synthesized phosphors, two devices were fabricated by combining 365 nm LED chips with Eu^{2+} solely (LED 1) and Eu^{2+}/Mn^{2+} co-doped (LED 2) BCKP, respectively. Comparing properties of LED1 and LED2, it is obviously observed that the device parameters of LED2 are better than those of LED1, which indicates that the introduction of Mn^{2+} in the phosphor effectively improve the property of LED devices due to the enhancement of red component in the spectrum. Figure 7b displays the emission spectrum of LED 2 together with the absorption spectra of the carotenoid and chlorophyll-b, and an obvious overlap was found between them. Results further indicate that the present sample BCKP: 1%Eu^{2+}, 20%Mn^{2+} not only can be effectively excite by n-UV LED chip to emit warm white light, but also can be used to promote the plant growth. In comparing traditional red and blue double band LEDs, the LEDs fabricated with present Eu^{2+}-Mn^{2+} co-doped BCKP phosphor are more appropriate for plant growth and offer more comfortable light environment for the operator.

4. Conclusions

In summary, a new family of compounds with representative compound $Ba_3CaK(PO_4)_3$ (BCKP) was synthesized *via* high-temperature solid-state reaction method, its structure was solved in direct space and refined by Rietveld method. Crystal structure possesses five cationic sites

including $Ba1O_9$, $Ba2O_{12}$, $Ba3O_9$, CaO_8 and KO_{10} on the base of the XRD Rietveld refinements. The phosphor BCKP: 1%Eu^{2+} emits a bright cold white light with about 90% QE and including five luminescent centers. Its complicated multi-luminescence centers were clearly assigned by low temperature spectra (LHT), TRES and the Van Uitert equation. The *first-principles calculations* was used to compute the *d*-orbital splitting energy to distinguish the assignment of peaks at 460 and 482 nm since Eu^{2+} at Ba1 or Ba3 sites has same CN and ionic radius. The emission centers of Eu^{2+} in crystallographic sites Ca, Ba1, Ba3, K and Ba2 are corresponded to the Gaussian fitting peaks at 430, 460, 481, 550 and 535 nm in BCKP: 1%Eu^{2+}, respectively. Additionally, the red component has been enhanced by introducing Mn^{2+} into BCKP: 1%Eu^{2+} and the QE of the co-doped sample remains 65%, and the ET process from Eu^{2+} to Mn^{2+} ions has been investigated in detail by photoluminescence spectra and decay curves. White LED devices were also fabricated by combining co-doped sample with 365 nm chip, which not only exhibits a excellent Ra (92) and CCT (4486 K) but also its spectra coincides well with the absorption spectra of the carotenoid and chlorophyll-b. Results indicate that the phosphor BCKP: Eu^{2+}, Mn^{2+} has great potential application in white LEDs and plant growth supplement lighting source.

Acknowledgments

This work was supported by National Natural Science Foundation of China (No. 11704312, 51672215, 11274251), Research Fund for the Doctoral Program of Higher Education of China (RFDP) (No.20136101110017) and by RFBR (17-52-53031).

Appendix A. Supplementary data

Supplementary data associated with this article can be found, in the online version.

References

[1] A. Agarwal, S. D. Gupta, Impact of light-emitting diodes (LEDs) and its potential on plant growth and development in controlled-environment plant production system, Curr. Biotechnol. 5 (2016) 28-43.

[2] M. Olle, A. Viršilė, The Effects of light-emitting diode lighting on greenhouse plant growth

and quality, Agric. food Sci. 22 (2013) 223-234.

[3] G. Tamulaitis, P. Duchovskis, Z. Bliznikas, K. Breivel, R. Ulinskaite, A. Brazaityte, A. Novikovas, A. Zukauskas, High-power light-emitting diode based facility for plant cultivation, J. Phys. D: Appl. Phys. 38 (2005) 3182-3187.

[4] A. Shimada, Y. Taniguchi, Red and blue pulse timing control for pulse width modulation light dimming of light emitting diodes for plant cultivation, J. Photoch. Photobio. B 104 (2011) 399–404.

[5] J. Y. Chen, N. M. Zhang, C. F. Guo, F. J. Pan, X. J. Zhou, H. Suo, X. Q. Zhao, E. M. Goldys, Site-dependent luminescence and thermal stability of Eu^{2+} doped fluorophosphate toward white LEDs for plant growth, ACS Appl. Mater. Interfaces 8 (2016) 20856-20864.

[6] Z. W. Zhou, J. M. Zheng, R. Shi, N. M. Zhang, J. Y. Chen, R. Y. Zhang, H. Suo, E. M. Goldys, C. F. Guo, Ab initio site occupancy and far-red emission of Mn^{4+} in cubic-phase $La(MgTi)_{1/2}O_3$ for plant cultivation, ACS Appl. Mater. Interfaces 9 (2016) 6177-6185.

[7] R. S. Liu, Phosphors, Up conversion nano particles, quantum dots and their applications, in: C. F. Guo, H. Suo (Eds.), Design of Single-phased Multicolor-emission Phosphor for LED, Springer Berlin, Heidelberg, 2017, pp. 459-508.

[8] L. Ma, D. J. Wang, Z. Y. Mao, Q. F. Lu, Z. H. Yuan, Investigation of Eu–Mn energy transfer in $A_3MgSi_2O_8$: Eu^{2+}, Mn^{2+} (A = Ca, Sr, Ba) for light-emitting diodes for plant cultivation, Appl. Phys. Lett. 93 (2008) 144101.

[9] C. F. Guo, X. Ding, L. Luan, Y. Xu, Two-color emitting of Eu^{2+} and Mn^{2+} co-doped $Sr_2Mg_3P_4O_{15}$ for UV LEDs, Sensor. Actuat. B 143 (2010) 712-715.

[10] A. Stockman, D. I. A. MacLeod, N. E. Johnson, Spectral sensitivities of the human cones, J. Opt. Soc. Am. A 10 (1993) 2491-2521.

[11] G. D. Massa, H. H. Kim, R. M. Wheeler, C. A. Mitchell, Plant productivity in response to LED lighting, HortScience 43 (2008) 1951-1956.

[12] Y. Sato, H. Kato, M. Kobayashi, T. Masaki, D. H. Yoon, M. Kakihana, Tailoring of deep-red luminescence in Ca_2SiO_4: Eu^{2+}, Angew. Chem., Int. Ed. 53 (2014) 7756-7759.

[13] H. P. Ji, Z. H. Huang, Z. G. Xia, M. S. Molokeev, V. V. Atuchin, M. H. Fang, Y. G. Liu, Discovery of new solid solution phosphors via cation substitution-dependent phase transition in $M_3(PO_4)_2$:Eu^{2+} (M = Ca/Sr/Ba) quasi-binary sets, J. Phys. Chem. C 119 (2015) 2038-2054.

[14] M. Y. Chen, Z. G. Xia, M. S. Molokeev, C. C. Lin, C. C. Su, Y. C. Chuang, Q. L. Liu, Probing Eu^{2+} luminescence from different crystallographic sites in $Ca_{10}M(PO_4)_7$:Eu^{2+} (M = Li, Na, and K) with β-$Ca_3(PO_4)_2$-type structure, Chem. Mater. 29 (2017) 7563-7570.

[15] C. H. Huang, Y. C. Chiu, Y. T. Yeh, T. S. Chan, T. M. Chen, Eu^{2+}-activated $Sr_8ZnSc(PO_4)_7$: a novel near-ultraviolet converting yellow-emitting phosphor for white light-emitting diodes, ACS appl. Mater. Interfaces 4 (2012) 6661-6668.

[16] Bruker, A. TOPAS, V4: General profile and structure analysis software for powder diffraction data; User's Manual; Bruker AXS: Karlsruhe, Germany, 2008.

[17] J. P. Perdew, K. Burke, M. Ernzerhof, Generalized gradient appromximate made simple, Phys. Rev. Lett. 77 (1996) 3865-3868.

[18] H. J. Monkhorst, J. D. Pack, Special points for brillouin-zone integrations, Phys. Rev. B 13 (1976) 5188-5192.

[19] *PLATON*–A multipurpose crystallographic tool; Utrecht University, Utrecht, The Netherlands, 2008.

[20] R. D. Shannon, Revised effective ionic radii and systematic studies of interatomic distances in halides and chalcogenides, Acta Crystallogr. A 32 (1976) 751-767.

[21] T. Naddari, H. El Feki, J. M. Savariault, Structure and ionic conductivity of the lacunary apatite $Pb_6Ca_2Na_2(PO_4)_6$, Solid State Ionics 158 (2003) 157-166.

[22] A. A. Belik, L. N. Ivanov, B. I. Lazoryak, V. B. Gutan, Synthesis, structure, and luminescence properties of $Ca_9MnM(PO_4)_7$ (M = Li, Na, K), Zhurnal Neorganicheskoj Khimii 46 (2001) 885-892.

[23] T. J. McCoy, I. M. Steele, K. Keil, B. F. Leonard, M. Endre, Chladniite, $Na_2CaMg_7(PO_4)_6$: a new mineral from the carleton (IIICD) iron meteroite, Am. Mineral. 79 (1994) 375-380.

[24] M. Kim, M. Kobayashi, H. Kato, H. Yamane, Y. Sato, M. Kakihana, Crystal structures and luminescence properties of Eu^{2+}-activated new $NaBa_{0.5}Ca_{0.5}PO_4$ and $Na_3Ba_2Ca(PO_4)_3$, Dalton Trans. 44 (2015) 1900-1904.

[25] Y. Yonesaki, C. Matsuda, Q. Dong, Structural consideration on the emission properties of Eu^{2+}-doped $Li_2BaMgP_2O_8$ and $Na_2BaMgP_2O_8$ orthophosphates, J. Solid State Chem. 196 (2012) 404-408.

[26] A. Boukhris, M. Hidouri, B. Glorieux, M. B. Amara, $Na_2BaMg(PO_4)_2$: synthesis, crystal

structure and europium photoluminescence properties, J. Rare Earth. 31 (2013) 849-856.

[27] K. Geng, Z. G. Xia, M. S. Molokeev, Crystal structure and luminescence property of a novel blue-emitting $Cs_{2x}Ca_{2x}Gd_{2(1-x)}(PO_4)_2$: Eu^{2+} (x = 0.36) phosphor, Dalton Trans. 43 (2014) 14092-14098.

[28] W. Z. Lv, Y. C. Jia, Q. Zhao, W. Lu, M. M. Jiao, B. Q. Shao, H. P. You, Synthesis, structure, and luminescence properties of $K_2Ba_7Si_{16}O_{40}$:Eu^{2+} for white light emitting diodes, J. Phys. Chem. C 118 (2014) 4649-4655.

[29] W. Z. Sun, Y. L. Jia, R. Pang, H. F. Li, T. F. Ma, D. Li, J. P. Fu, S. Zhang, L. H. Jiang, C. Y. Li, $Sr_9Mg_{1.5}(PO_4)_7$: Eu^{2+}: a novel broadband orange-yellow-emitting phosphor for blue light-excited warm white LEDs, ACS Appl. Mater. Interfaces 7 (2015) 25219-25226.

[30] A. L. Companion, M. A. Komarynsky, Crystal field splitting diagrams, J. Chem. Educ. 41 (1964) 257-262.

[31] P. A. Tanner, L. X. Ning, Electronegativity, charge transfer, crystal field strength, and the point charge model revisited, J. Phys. Chem. A 117 (2013) 1503-1507.

[32] K. S. Sohn, S. J. Lee, R. J. Xie, N. Hirosaki, Time-resolved photoluminescence analysis of two-peak emission behavior in $Sr_2Si_5N_8$: Eu^{2+}, Appl. Phys. Lett. 95 (2009) 121903.

[33] C. Grieco, K. F. Hirsekorn, A. T. Heitsch, A. C. Thomas, M. H. McAdon, B. A. Vanchura, M. M. Romanelli, L. L. Brehm, A. Leugers, A. Sokolov, J. B. Asbury, Mechanisms of energy transfer and enhanced stability of carbidonitride phosphors for solid state lighting, ACS Appl. Mater. Interfaces 9 (2017) 12547-12555.

[34] J. Stöhr, H. C. Siegmann, Magnetism: from fundamentals to nanoscale dynamics, Springer Science & Business Media, 2007.

[35] X. J. Zhang, J. Wang, L. Huang, F. J. Pan, Y. Chen, B. F. Lei, M. Y. Peng, M. M. Wu, Tunable luminescence properties and concentration-dependent, site-preferable distribution of Eu^{2+} ions in silicate glass for white LEDs applications, ACS Appl. Mater. Interfaces 7 (2015) 10044-10054.

[36] D. L. Dexter, J. H. Schulman, Theory of concentration quenching in inorganic phosphors, J. Chem. Phys. 22 (1954) 1063-1070.

[37] M. C. Wu, C. Y. Hou, C. M. Jiang, Y. T. Wang, C. Y. Wang, H. H. Chen, H. M. Chang, A novel approach of LED light radiation improves the antioxidant activity of pea seedlings, Food Chem. 101 (2007) 1753–1758.

[38] H. Suo, C. F. Guo, Z. Yang, S. S. Zhou, C. K. Duanb, M. Yin, Thermometric and optical heating Bi-functional properties of upconversion phosphor $Ba_5Gd_8Zn_4O_{21}$:Yb^{3+}/Tm^{3+}, J. Mater. Chem. C 3 (2015) 7379-7385.

[39] K. Li, J. Fan, M. M. Shang, H. Z. Lian, J. Lin, $Sr_2Y_8(SiO_4)_6O_2$: Bi^{3+}/Eu^{3+}: a single-component white-emitting phosphor via energy transfer for UVw-LEDs, J. Mater. Chem. C 3 (2015) 9989-9998.

[40] J. Chen, Y. G. Liu, M. H. Fang, Z. H. Huang, Luminescence properties and energy transfer of Eu/Mn-coactivated $Mg_2Al_4Si_5O_{18}$ as a potential phosphor for white-light LEDs, Inorg. Chem. 53 (2014) 11396-11403.

[41] Y. J. Zheng, H. M. Zhang, H. R. Zhang, Z. G. Xia, Y. L. Liu, M. S. Molokeev, B. F. Lei, Co-substitution in $Ca_{1-x}Y_xAl_{12-x}Mg_xO_{19}$ phosphors: Local structure evolution, photoluminescence tuning and application for plant growth LEDs, J. Mater. Chem. C 6 (2018) 4217-4224.

[42] Y. W. Zhu, L. Y. Cao, M. G. Brik, x. J. Zhang, L. Huang, T. T. Xuan, J. Wang, Facile synthesis, morphology and photoluminescence of a novel red fluoride nanophosphor K_2NaAlF_6: Mn^{4+}, J. Mater. Chem. C 5 (2017) 6420-6426.

Figure and Table captions

Figure 1. Rietveld refinement XRD patterns of blank BCKP (a) as well as BCKP: 1%Eu^{2+}, 20%Mn^{2+} (b) together with crystal structure of the BCKP host and cationic sites (c).

Figure 2. The PL and PLE spectra (a) and the normalized two-dimensional time-resolved emission spectra (TRES) (b) together with the normalized spectra slices of TRES at 1.0, 1.5, 2.5, 4.5 μs (c) of the 1%Eu^{2+} doped BCKP at room temperature.

Figure 3. The PL spectrum of BCKP: Eu^{2+} at liquid helium temperature with the Gaussian fitting peaks and five cationic sites.

Figure 4. The optimized structure of BCKP and the projector density of states (PDOS) of the *d*-orbital splitting energy level of Eu^{2+} doped into Ba1 (a, c) or Ba3 (b, d) site.

Figure 5. (a) Temperature-dependent two-dimensional photoluminescence spectrum (λ_{ex} = 365 nm), (b) integrated PL intensity and (c) activation energy of thermal quenching of BCKP: 1%Eu^{2+}. The inset shows the schematic configuration coordinate diagram of the Eu^{2+} ion.

Figure 6. (a) PLE and PL spectra of (a) 1%Eu^{2+}, (b) 10%Mn^{2+} and (c) 1%Eu^{2+}, 20%Mn^{2+} doped BCKP; (d) the decay time of BCKP: 1%Eu^{2+}, *y*%Mn^{2+} (*y* = 0, 5, 10, 15, 20) and the inset shows ET efficiency from Eu^{2+} to Mn^{2+} with different contents of Mn^{2+}.

Figure 7. The chromaticity coordinates of two white LED devices fabricated by combining 365 nm chips with phosphors BCKP: 1%Eu^{2+} (No.1) and BCKP: 1%Eu^{2+}, 20%Mn^{2+} (No.2) (a) together with the emission spectra of No.2 white LED device along with the absorption spectra of carotenoid and chlorophyll-b (b).

Table 1. Rietveld refinement and crystallographic parameters of BCKP and BCKP: 1%Eu^{2+}, 20%Mn^{2+}.

Figures and Table

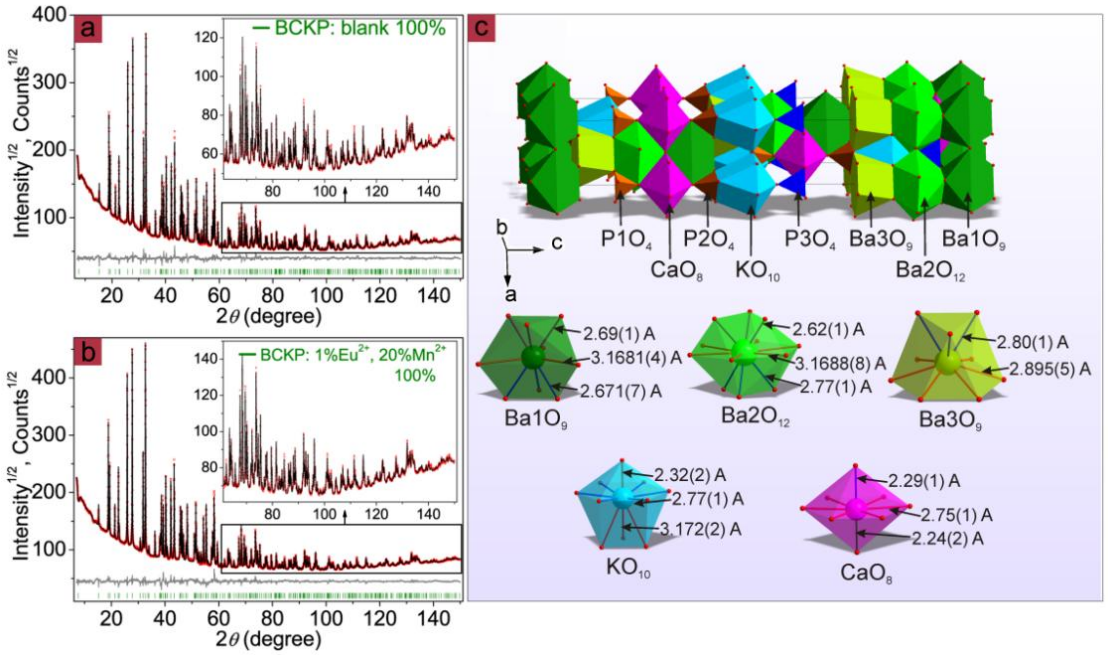

Figure 1. Rietveld refinement XRD patterns of blank BCKP (a) as well as BCKP: 1%Eu^{2+}, 20%Mn^{2+} (b) together with crystal structure of the BCKP host and cationic sites (c).

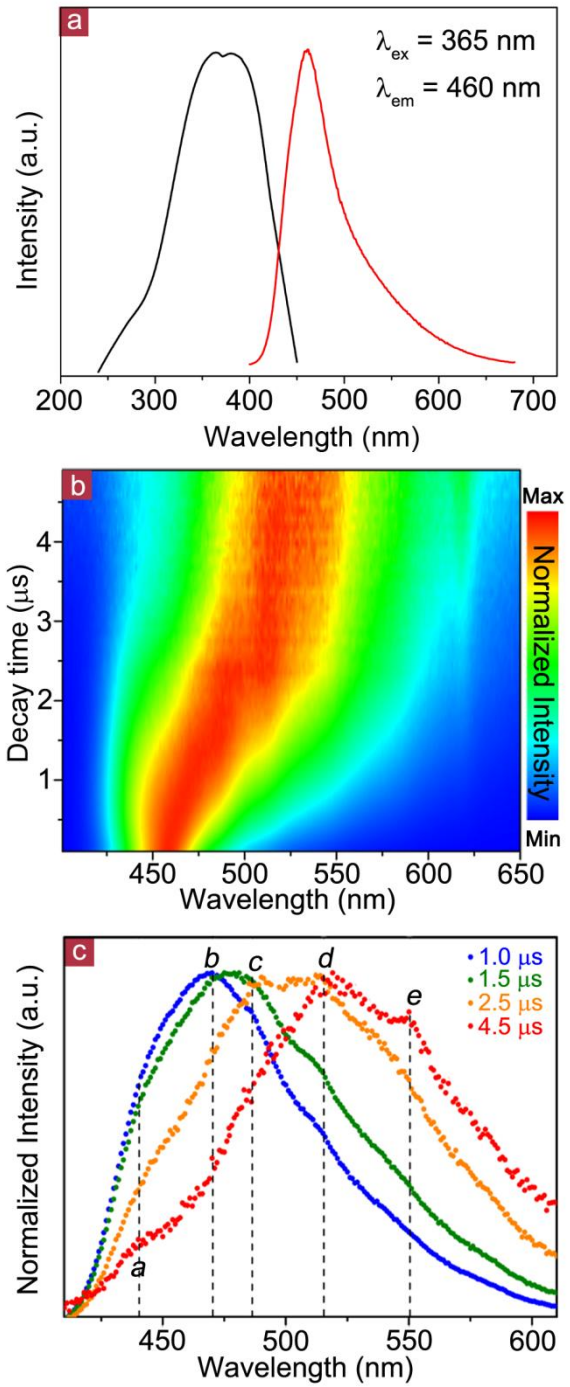

Figure 2. The PL and PLE spectra (a) and the normalized two-dimensional time-resolved emission spectra (TRES) (b) together with the normalized spectra slices of TRES at 1.0, 1.5, 2.5, 4.5 μs (c) of the 1%Eu^{2+} doped BCKP at room temperature.

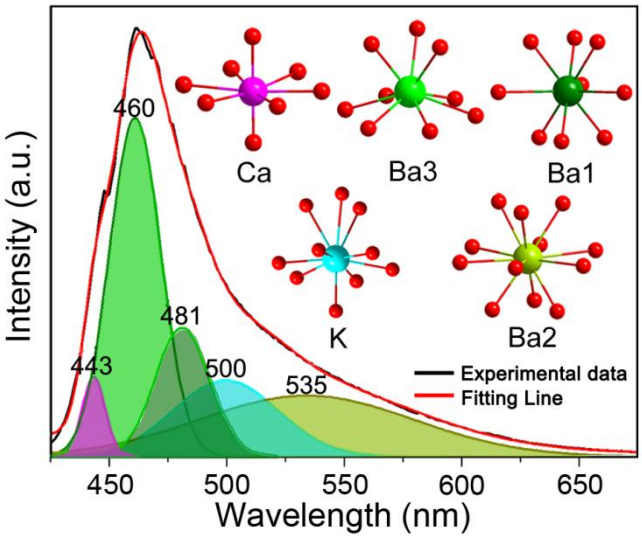

Figure 3. The PL spectrum of BCKP: Eu^{2+} at liquid helium temperature with the Gaussian fitting peaks and five cationic sites.

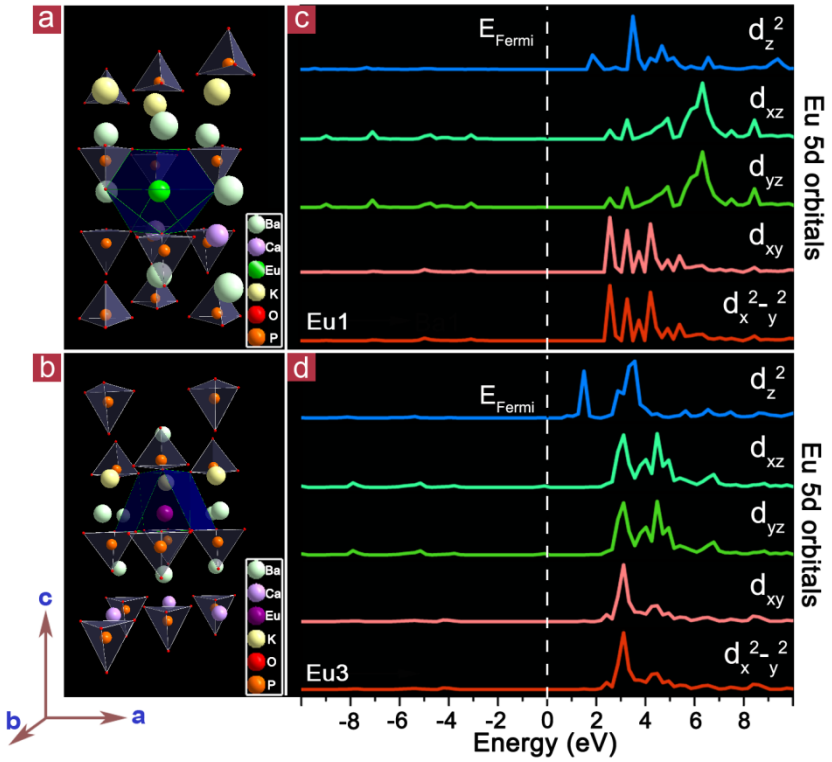

Figure 4. The optimized structure of BCKP and the projector density of states (PDOS) of the *d*-orbital splitting energy level of Eu^{2+} doped into Ba1 (a, c) or Ba3 (b, d) site.

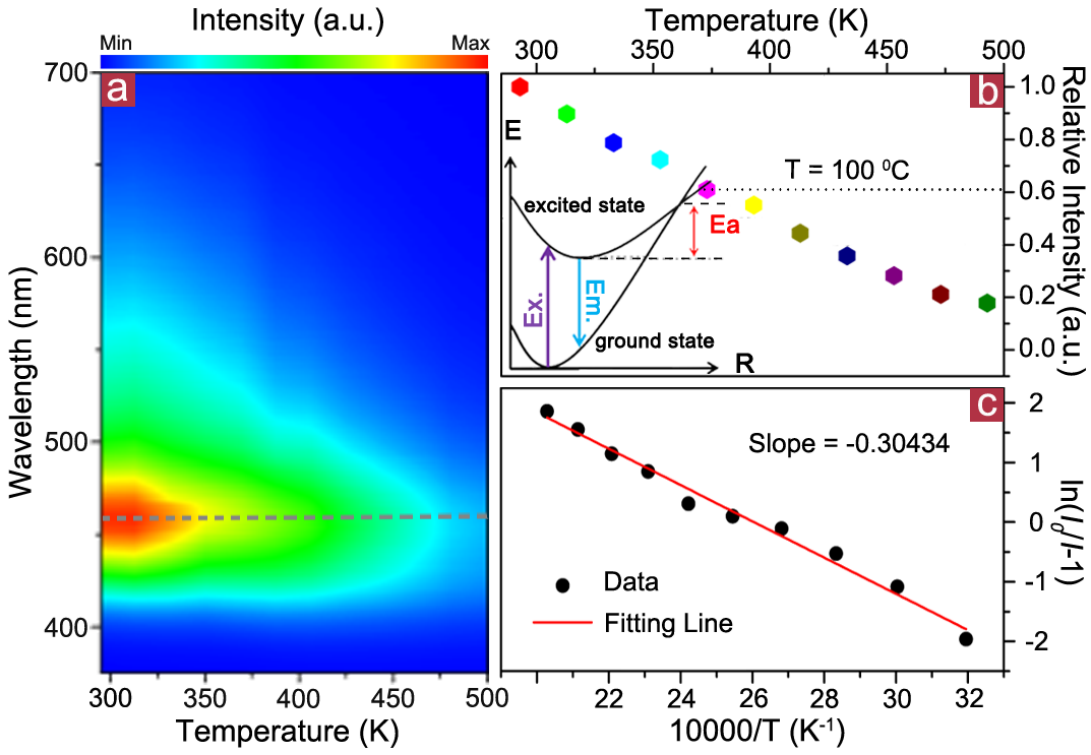

Figure 5. (a) Temperature-dependent two-dimensional photoluminescence spectrum (λ_{ex} = 365 nm), (b) integrated PL intensity and (c) activation energy of thermal quenching of BCKP: 1%Eu^{2+}. The inset shows the schematic configuration coordinate diagram of the Eu^{2+} ion.

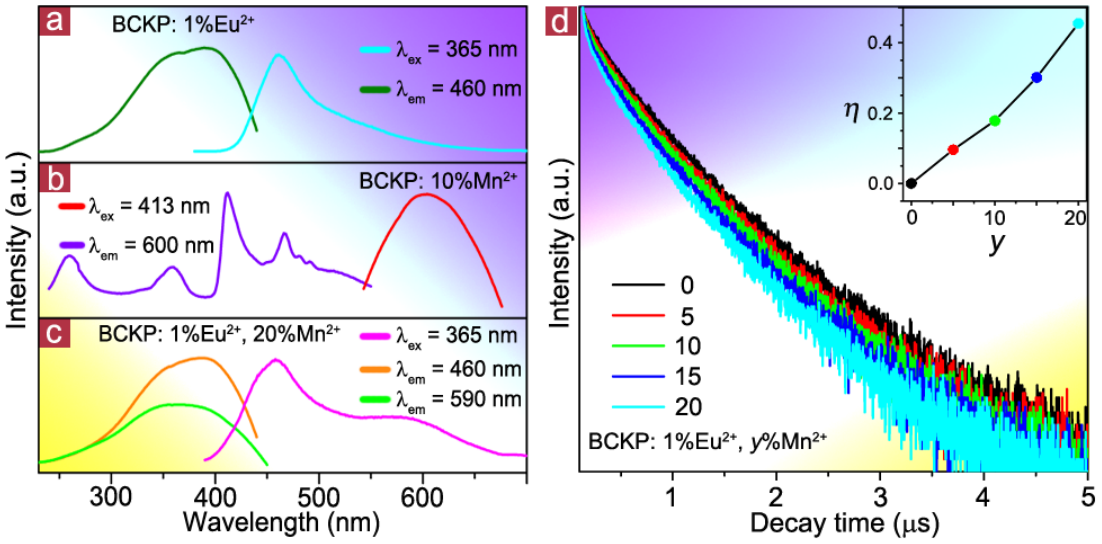

Figure 6. (a) PLE and PL spectra of (a) 1%Eu^{2+}, (b) 10%Mn^{2+} and (c) 1%Eu^{2+}, 20%Mn^{2+} doped BCKP; (d) the decay time of BCKP: 1%Eu^{2+}, *y*%Mn^{2+} (*y* = 0, 5, 10, 15, 20) and the inset shows ET efficiency from Eu^{2+} to Mn^{2+} with different contents of Mn^{2+}.

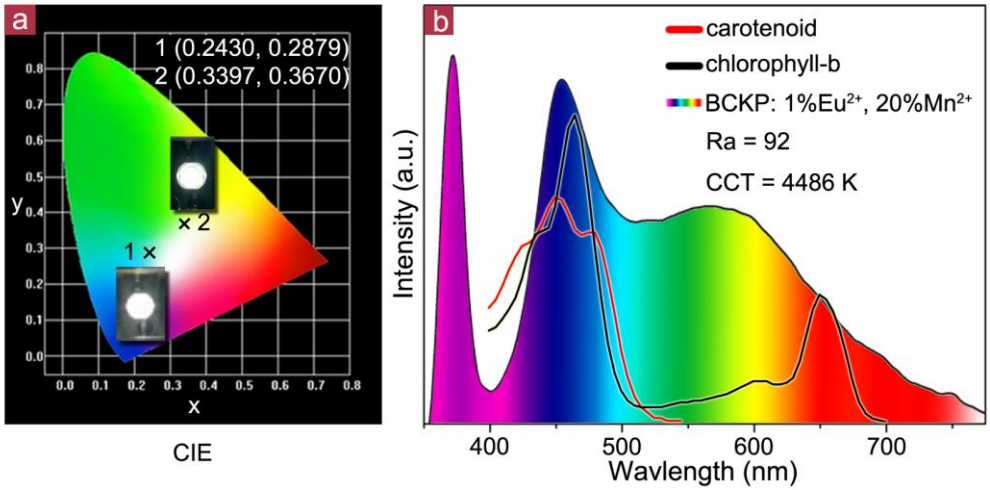

Figure 7. The chromaticity coordinates of two white LED devices fabricated by combining 365 nm chips with phosphors BCKP: 1%Eu^{2+} (No.1) and BCKP: 1%Eu^{2+}, 20%Mn^{2+} (No.2) (a) together with the emission spectra of No.2 white LED device along with the absorption spectra of carotenoid and chlorophyll-b (b).

Table 1. Rietveld refinement and crystallographic parameters of BCKP and BCKP: 1%Eu^{2+}, 20%Mn^{2+}.

Compound	**BCKP**	**BCKP: 1%Eu^{2+}, 20%Mn^{2+}**
space group	*R*3*m*	*R*3*m*
***a*, Å**	5.48501 (8)	5.48114 (3)
***c*, Å**	34.9204 (5)	34.9175 (2)
***V*, Å^3**	909.84 (3)	908.48 (1)
Z	3	3
***2θ*-interval, °**	7-150	7-150
R_{wp}, %	3.46	3.26
R_p, %	2.75	2.61
R_{exp}, %	0.94	0.76
χ^2	3.68	4.29
R_B, %	2.94	2.55

Graphical abstract

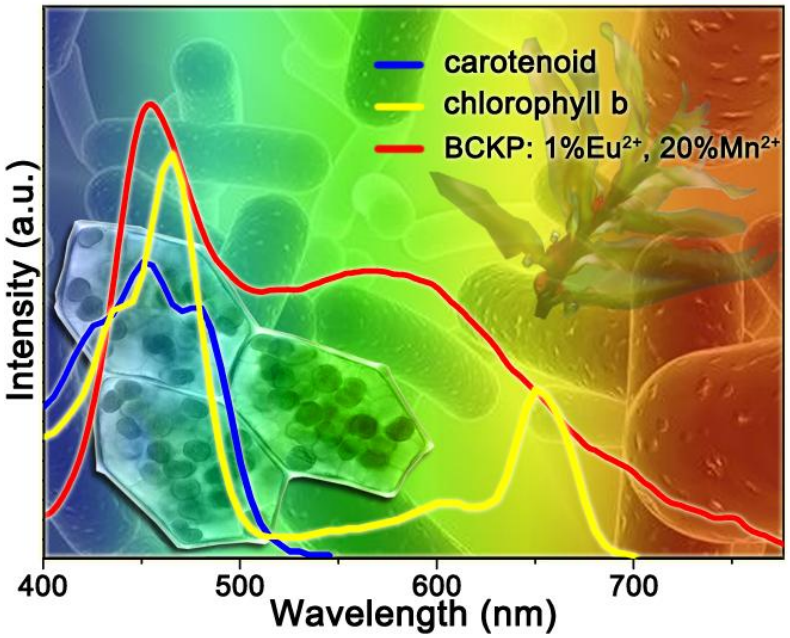

Enhancement of Red Emission and Site Analysis in Eu^{2+} Doped New-Type Structure $Ba_3CaK(PO_4)_3$ for Plant Growth White LEDs

Jinmeng Xiang[†], Jiming Zheng[†], Ziwei Zhou[†], Hao Suo[†], Xiaoqi Zhao[†], Xianju Zhou[#], Niumiao Zhang[†], Maxim S. Molokeev[‡, Δ, ⊥*] and Chongfeng Guo[†*]

[†] *National Key Laboratory of Photoelectric Technology and Functional Materials in Shaanxi Province, National Photoelectric Technology and Functional Materials & Application of Science and Technology International Cooperation Base, Institute of Photonics & Photon-Technology and Department of Physics, Northwest University, Xi'an 710069, China*

[#] *School of Science, Chongqing University of Posts and Telecommunications, Chongqing, 400065, P. R. China*

[‡] *Laboratory of Crystal Physics, Kirensky Institute of Physics, Federal Research Center KSC SB RAS, Krasnoyarsk 660036, Russia*

[Δ] *Siberian Federal University, Krasnoyarsk, 660041, Russia*

[⊥] *Department of Physics, Far Eastern State Transport University, Khabarovsk, 680021 Russia*

Corresponding authors

**E-mail: guocf@nwu.edu.cn (Prof. Guo)*

msmolokeev@mail.ru (Prof. Molokeev)

Abstract

A novel compound $Ba_3CaK(PO_4)_3$ (BCKP) with new-type structure was synthesized and its structure was determined by X-ray diffraction Rietveld refinement, in which crystal structure consists of $Ba1O_9$, $Ba2O_{12}$, $Ba3O_9$, CaO_8 and KO_{10} polyhedra, that's five cationic sites. As a phosphor host, Eu^{2+} doped BCKP emits cold white light with about 90% quantum efficiency (QE) through entering different cationic sites. Based on the results of refinement, three Eu^{2+} luminescence centers in sites Ca, Ba2 and K were clearly assigned in Eu^{2+} solely doped BCKP by the time-resolved emission spectra (TRES), Van Uitert equation, but the emissions of Eu^{2+} at Ba1 and Ba3 sites are not easy to be determined for the same coordination number (CN). According to their different spatial distribution of the coordinated atoms, the *first-principles calculation* was used to compute the *d* orbital splitting energy of Eu^{2+} ions in Ba1 and Ba3 sites to accurately distinguish the ambiguous luminescence centers. In order to meet the requirement of plant growth

spectra, Mn^{2+} was introduced into BCKP: Eu^{2+} to enhance the red component of spectra, which not only perfectly match with the absorption spectra of carotenoid and chlorophyll-b, but also LEDs fabricated through combining 365 nm near ultraviolet (n-UV) chip with BCKP: Eu^{2+}, Mn^{2+} phosphor exhibit excellent parameters including high color rendering index (Ra) (92), excellent correlated color temperature (CCT) (4486 K) and outstanding QE up to 65%. Results confirmed that BCKP: Eu^{2+}/Mn^{2+} phosphor with great potential applications in white LEDs and plant growth.

Keywords: Phosphor; $Ba_3CaK(PO_4)_3$; Sites-dependent photoluminescence; Plant growth; White LEDs

1. Introduction

Light not only affects the overall growth rhythm and development processes of plants, but also offers the energy source for plant cultivation. The artificial light supplement becomes necessary and popular for increasing production and quality or guiding the rhythm of plant in conventional indoor agriculture/horticulture and a short growing season or high latitude area with poor light [1, 2]. Red (600-700 nm) and blue (400-500 nm) light are dominant and responsible for phototropism and photosynthesis in the process of plant growth, respectively, which imply that it is more efficient for the artificial lighting with the capability of spectral composition control [3, 4]. Obviously, traditional artificial lighting sources cold-cathode fluorescent lamps (CCFLs) and gas discharge lamps (GDLs) suffer the serious mismatch between their emission spectra and the absorption of the main pigments chlorophylls and carotenoids in the process of photosynthesis [5]. Thus, light-emitting diodes (LEDs) used in modern agriculture as supplementary lighting source have been developed rapidly in recent decades due to their high light output with low radiant heat and controllable spectral composition [6]. Phosphor-converted light-emitting diodes (pc-LEDs) with mature fabrication technique are the most popular, in which several single-color emitting phosphors were excited by near-ultraviolet (n-UV) or blue LED chips and the true spectral composition control could be realized through adjusting the component of phosphors. In order to low the cost and enhance efficiency of pc-LEDs, it is necessary to avoid the re-absorption and different aging rate between each phosphor [7]. Single-phased multicolor-emitting phosphor is an ideal choice for dissolving above mentioned problems, and some phosphors with well-matched

double-emission band have been designed for plant growth LED based on energy transfer, such as Eu^{2+}, Mn^{2+} co-doped $A_3MgSi_2O_8$ (A = Ca, Sr, Ba) [8] and $Sr_2Mg_3P_4O_{15}$ [9] with strong blue and red emission. However, recent investigations illuminated that white light environment not only make operators worked in the green house comfortable [10], but also let plants grow better than those in blue plus red light environment on the premise of the matched emission wavelengths with photosynthetic active radiation [11].

For the phosphors used in plant growth lighting sources, the broad band emissions are perfect and well matched with the absorption spectra of plant growth pigments. Eu^{2+} doped phosphors usually offer a broad band emission due to its typical 4f-5d transitions and cold white light emission phosphor doped with Eu^{2+} have been developed in our group, in which site-dependent emission from the Eu^{2+} varied with the crystal field strength of the occupied cationic sites [12]. It is possible to search for a phosphor for plant growth LED through doping Eu^{2+} in a host with several cationic sites. Phosphate compounds with β-$Ca_3(PO_4)_2$-type structure are attractive phosphor hosts due to their versatile structural types and substation-induced tunable composition, in which there are five Ca^{2+} sites. Its formula could also be written as β-$Ca_{3n}(PO_4)_{2n}$ (n=1, 2, 3…) and Ca^{2+} can be partially substituted to construct more new phases with β-$Ca_3(PO_4)_2$-type, such as two univalent metal M^+ ions substitute one Ca^{2+} ion, two trivalent metal ions R^{3+} substitute three Ca^{2+} ions or one divalent metals ions substitute one Ca^{2+} ion, leading to a large number of new compounds $A_3(PO_4)_2$ (A = Ca, Sr, Ba) [13], $A_{10}M(PO_4)_7$ (A = Ca, Sr, Ba; M = Li, Na, K) [14] and $A_9R(PO_4)_7$ (A = Ca, Sr, Ba; R = Cr and rare earth) [15]. For Eu^{2+} doped phosphor with β-$Ca_3(PO_4)_2$-type structure, its emission spectrum could be effectively tuned through entering different sites because Eu^{2+} ions with f-d transition suffer different crystal field. The compound under investigation, $Ba_3CaK(PO_4)_3$ was achieved through six Ba^{2+} and two K^+ replace of six Ca^{2+} and one Ca^{2+} in β-$Ca_9(PO_4)_6$, respectively, to form the compound $Ba_6Ca_2K_2(PO_4)_6$, namely $Ba_3CaK(PO_4)_3$. However, the present cation replacement absolutely led to a new crystal structure, which was not determined yet and has never been discussed.

Here, the detailed structure of host material $Ba_3CaK(PO_4)_3$ (BCKP) was determined in real space by Monte-Carlo method with simulated annealing procedure and after that refined by Rietveld method, and the site-dependent spectra analysis of Eu^{2+} in the BCKP host was also investigated through photoluminescence at liquid helium temperature (LHT), time-resolved

emission spectra (TRES) and *first-principle calculation*. Eu^{2+} solely-doped sample displayed a cold white emission with outstanding QE (90%) under the near ultraviolet (n-UV) light excitation, Mn^{2+} ions were introduced to enhance the red spectral components through efficient energy transfer from Eu^{2+} to Mn^{2+} ions in order to match well with the absorption spectra of carotenoid and chlorophyll-b. The white LED devices with excellent Ra (92), CCT (4486 K) and QE (65%) have been fabricated by combining the 365 nm chip with the Eu^{2+}-Mn^{2+} co-doped BCKP, which is not only can be used for plant growth white LEDs, but also can make operators worked in indoor agriculture comfortable.

2. Material and methods

2.1. Synthesis and characterization.

A series of Eu^{2+} singly and Eu^{2+}-Mn^{2+} co-doped $Ba_3CaK(PO_4)_3$ (BCKP) were prepared *via* convenient high-temperature solid-state reaction method, in which analytical reagent (A. R.) $CaCO_3$, $BaCO_3$, K_2CO_3, $NH_4H_2PO_4$, $MnCO_3$ and high purity Eu_2O_3 (99.99%) were used as starting materials. The stoichiometric amount of raw materials was mixed thoroughly with appropriate volume ethanol in an agate mortar and then dried at 70℃ for 1 h. After that the dried the mixture was pre-sintered at 600 ^oC for 3 h, next to further calcine at 1250 ^oC for 8 h in CO reducing atmosphere to obtain the final products.

The structure and purity of samples were determined by powder X-ray diffraction (XRD), and the diffraction data of host material BCKP and BCKP: 1%Eu^{2+}, 20%Mn^{2+} for structural solving and Rietveld analysis were collected with a Bruker D8 ADVANCE powder diffractometer (Cu-$K\alpha$ radiation) and linear VANTEC detector at room temperature. The step size of 2θ was set as 0.016°, and the counting time was 10 and 15 s per step for BCKP and BCKP: 1%Eu^{2+}, 20%Mn^{2+}, respectively. The 2θ in range of 7-70º was measured with 0.6 mm divergence slit, but 2θ ranging 70-150º was measured with 2 mm divergence slit. Larger slits allow noticeable increase of intensity in high-angle peaks without loss of resolution because the high-angle peaks were broad enough to be not affected by bigger divergence beam. The esd's $\sigma(I_i)$ of all points on patterns were calculated using intensities I_i: $\sigma(I_i) = I_i^{1/2}$. The intensities and obtained esd's were further normalized: $I_{i\ norm} = I_i \times 0.6/(\text{slit width})$, $\sigma_{norm}(I_i) = \sigma(I_i) \times 0.6/(\text{slit width})$, taking into

account actual value of divergence slit width used to measure each particular intensity I_i and saved in xye-type file. So transformed powder pattern usually had view in whole 2θ range 5-140°, all high-angle points had small esd's. The crystal structure refinement was performed by using TOPAS 4.2 [16], in which each point of esd's was accounted by special weight scheme.

The photoluminescence emission (PL) and excitation (PLE) spectra at liquid helium temperature (LHT), temperature-dependent spectra, time-resolved emission spectra (TRES) as well as PL decay curves were measured on an Edinburgh FLS920 spectrophotometer equipped with a 450 W Xe lamp as the excitation source for the steady state spectra and an EPL-375 pulse laser as the pumping source for decay curves. An Oxford OptistatDN2 nitrogen cryogenics and CTI-Cryogenics temperature controlling system (with about 20 min duration time at the fixed temperature) were attached with FLS920 spectrometer to measure the temperature-dependent luminescent properties. The quantum efficiency (QE) was tested on the Quantaurus QY (C9920-02G, Japan) spectrometer.

2.2. Computation.

The *first-principle calculations* were performed within the framework of density functional theory (DFT), which was implemented in the *Vienna ab initio simulation package* (VASP). The exchange correlation was carried out using the generalized gradient approximation (GGA) *Perdew-Burke-Ernzerhof* (PBE) and the projector augmented wave (PAW) method potentials [17]. The plane-wave cutoff energy was set below 500 eV and the Brillouin zone was sampled with *Γ*-centered k-meshes of 12 × 12 × 2 on the basis of the Monkhorst and Pack (MP) method [18]. The optimized structures were established by *ab-initio computation*, in which the total energy convergence threshold of the unit cell was less than 10^{-5} eV/atom and the residual atomic forces was smaller than 10^{-3} eV/Å. A 2 ×2 × 1 supercell with 240 atoms was constructed using the structure of BCKP with *R3m* space group, in which twelve Ba1 and Ba3 were coordinated by nine oxygen atoms but their spatial distribution is different. Then single Ba1 or Ba3 was substituted by a Eu atom and the density of state (DOS) was calculated to analyze the luminescent properties according to their crystal environment and *d* orbital splitting. The detailed discussion would be given in the following part.

3. Results and discussion

3.1. XRD refinement of samples.

All peaks of $Ba_3CaK(PO_4)_3$ (BCKP) pattern were indexed by trigonal *R*-centered unit cell with parameters a = 5.4784 Å, c = 34.9043 Å, V = 907.24 $Å^3$ (GOF = 111.22). The most probable space groups are *R*3, *R*-3, *R*3*m*, *R*32 and *R*-3*m*. The structure solving in the lowest space groups, *R*3 will account for all possible solutions in higher space groups, therefore, it was initially decided to solve the structure in the *R*3 space group. The program TOPAS 4.2 [16] was used to solve the crystal structure. The charge flipping procedure and Patterson synthesize were used to localize heavy ions. It was clearly found that all big maximums of electron density are located in the *c*-axis. Taking into account the average volume of non-hydrogen ion is 17 $Å^3$, it was calculated that asymmetric unit cell contains $V/(17Å^3 \times Z)$ = 907.24 Å/(17 Å × 3) ≈ 18 ions. Formula $Ba_3CaK(PO_4)_3$ gives 20 ions and it was decided that three Ba^{2+}, one Ca^{2+}, one K^+ and three PO_4^{3-} ions are located in the *c*-axis. The structure was solved using a simulated annealing procedure to the randomized *z*-coordinates of two Ba^{2+} ions, one Ca^{2+}, one K^+ and three P^{5+} ions, the *x*, *y* coordinates of these ions were equal to 0 during solving. Moreover third Ba^{2+} ion was placed in (0, 0, 0) site and it was *z*-coordinated ion. So, it was totally used only 8 parameters. The dynamical occupancy correction of the atoms wasn't used. After the calculations, a solution was found with R_{wp} = 9.8%, R_B = 9.3%. Then, the Rietveld refinement was performed and the difference electron density based of F_{obs}-F_{calc} difference of the structural amplitudes revealed all O^{2-} ions near P^{5+} ions so that three PO_4 tetrahedra were formed. The structural analysis of $Ba_3CaK(PO_4)_3$ using the program PLATON [19] revealed additional element of symmetry, *m* plane, and the space group was changed to *R*3*m*. all O^{2-} ions were placed in the closest special sites and new cycle of refinement was performed. The R-factors rapidly dropped down R_{wp} = 6.63% and R_B = 6.04%. The final Rietveld refinement accounts spherical harmonic 2 order of preferred orientation, surface roughness. Isotropic thermal parameters of all ions were refined independently besides O^{2-} ions, which have only one thermal parameter in order to reduce number of refined parameters. Refinement was stable and gives low *R*-factors (Table 1, Figure 1a). Coordinates of atoms and main bond lengths are in Table S1 and Table S2, respectively.

Crystal structure $Ba_{2.97}Eu_{0.03}Ca_{0.8}Mn_{0.2}K(PO_4)_3$ was refined using model of $Ba_3CaK(PO_4)_3$,

all Ba sites were doped by Eu^{2+} ions and Ca sited was doped by Mn^{2+} according to suggested chemical formula. The concentration values were not refined due to low Eu^{2+} concentration and due to similarity of Ca and Mn atomic scattering functions. Refinement was also stable and gives low *R*-factors (Table 1, Figure 1b). Coordinates of atoms and main bond lengths are in Table 1S and Table 2S, respectively. It was found that cell volume of $Ba_{2.97}Eu_{0.03}Ca_{0.8}Mn_{0.2}K(PO_4)_3$ V = 908.48(1) Å3 is smaller than V = 909.74(3) $Å^3$ of $Ba_3CaK(PO_4)_3$ which is consistent with smaller ion radii (IR) of Mn IR(Mn^{2+}, CN = 8) = 0.96 Å in comparison with IR(Ca^{2+}, CN = 8) = 1.12 Å, and with smaller ion radii of Eu IR(Eu^{2+}, CN = 9) = 1.3 Å in comparison with IR(Ba^{2+}, CN = 9) = 1.47 Å [20]. All XRD patterns of the prepared samples are similar and depicted in Figure S1, which further confirm that Eu^{2+} and Mn^{2+} enter into the host successfully.

Cell parameter search in the ICSD database (Version 2018-1) didn't reveal any isostructural or similar compounds to $Ba_3CaK(PO_4)_3$. Compound with similar chemical formula $Pb_3CaNa(PO_4)_3$ (lacunary apatite) [21] has *P*63/*m* space group, another cell parameters and of course absolutely another crystal structure. Crystal structure $Ba_3CaK(PO_4)_3$ (Figure 1c) consists of BaO_9, BaO_{12}, CaO_8, KO_{10} polyhedra connected by vertexes, edges and faces forming 3D net, the tetrahedra voids between large polyhedra are filled by PO_4 tetrahedra. It is interesting that all polyhedra lie on the 3-fold axis and have high local symmetry with point symbol 3*m*, and this is noticeable different with structures $Ca_9MMn(PO_4)_7$ (M = Li, Na, K) (*R*3*c*) [22], $Na_2CaMg_7(PO_4)_7$ (chladniite) [23]. Crystal structure $Ba_2CaNa_3(PO_4)_3$ (*P*31*c*) [24], which can be obtained from $Ba_3CaK(PO_4)_3$ by changing $Ba^{2+} \rightarrow 2Na^+$, has (Ca/Na)$O_6$, BaO_9, BaO_{12} polyhedra on the 3-fold axis, but their local symmetry are only 3. It should be noted that in spite of crystal structures of $Ba_2CaNa_3(PO_4)_3$ and $Ba_3CaK(PO_4)_3$ are different and *c* cell parameters are also different, they have similar cell parameters *a* = 5.4515(2) and *a* = 5.48501(8) Å, respectively. Crystal structure $BaMgNa_2(PO_4)_2$ [25, 26] has only one Ba site with local symmetry -3 [25] or -3*m* [26] and this compound is centrosymmetric, but compound under consideration $Ba_3CaK(PO_4)_3$ is polar. Compound $Gd_2CaCs(PO_4)_3$ ($P6_222$) [27], which can be obtained from $Ba_3CaK(PO_4)_3$ by changing $3Ba^{2+} \rightarrow 2Gd^{3+}$ and $K^+ \rightarrow Cs^+$, consists of CsO_8 and (Gd, Ca)O_8 square antiprisms with local symmetry 222. So, compound $Ba_3CaK(PO_4)_3$ is new polar compound with unique set of Ba-Ca-K polyhedra possessing the highest local structure 3*m* among all polar trigonal compounds.

3.2. Sites-dependent PL spectra.

According to above crystal structure results, Eu^{2+} ions have chance to enter five different cationic sites in BCKP host, which make it reasonable to have five emission bands for BCKP: Eu^{2+} due to its crystal field strength dependent emission. Figure 2a displays the PL and PLE spectra of BCKP: 1%Eu^{2+} at room temperature, in which a broad and strong excitation band monitoring at 460 nm was observed in the range of 250 to 440 nm and the PLE spectrum matches well with the commercial n-UV LED chip. The present sample shows bright cold white light emission with an unsymmetrical band ranging from 400 to 675 nm under the excitation of 365 nm light, which hints that there are more than one luminescence centers in BCKP: 1%Eu^{2+} and its QE is about 90%. As mentioned above, Eu^{2+} ions can enter five cationic sites, in which different crystal field environments lead to the diverse emission wavelengths and lifetimes for Eu^{2+} ions.

To further prove the existence of multiple sites of Eu^{2+} and determine the number of luminescence centers, the normalized time-resolved emission spectra (TERS) of sample BCKP: 1%Eu^{2+} were measured at room temperature with the excitation of 375 nm EPL pulse laser, as shown in Figure 2b and c. A significant red-shift was observed in the two-dimensional TRES (in Figure 2b), implying the existence of multiple luminescence centers. No obvious shift was observed in the emission peak at the decay time ranging from 0 to 1 μs and 3 to 4.5 μs; whereas the maximum emission peak rapidly shift from 460 to 520 nm with decay time growing from 1.0 to 3.0 μs. Four representative normalized TRES at specific time 1.0, 1.5, 2.5 and 4.5 μs were used to confirm the accurate number of those luminescent centers, as shown in Figure 2c. Peak *b* in TRES was first detected at 1 μs; then peaks *c* and *d* gradually appeared with prolonging the time from 1 to 2.5 μs and the peaks *a* and *e* become clear with delaying the time to 4.5 μs. This result indicated the existence of five luminescence centers, which is contributed to five cationic sites occupied by activator Eu^{2+} ions.

The precise assignment of luminescent center emission position is difficult to identify at room temperature because of thermal vibration, thus the PL spectrum of Eu^{2+} doped BCKP at liquid helium temperature (LHT) was displayed in Figure 3 under the 365 nm n-UV light excitation. An asymmetric broad emission band ranging from 400 to 700 nm was observed in the PL spectrum, which could attribute to the typical emission of Eu^{2+} 5d → 4f transitions from different sites. The PL spectrum at LHT could be well fitted by the sum of five Gaussian peaks, bands centered at 443, 460, 481, 500 and 535 nm, respectively. Insets of Figure 3 give the

polyhedron of each cationic site. In order to assign the relationship between the luminescence centers and cationic sites, the Van Uitert equation is used to approximate estimate emission position of Eu^{2+} at five different cites: [28, 29]

$$E = Q\left[1-\left(\frac{V}{4}\right)^{\frac{1}{V}}\times 10^{-\frac{nEar}{80}}\right] \quad (1)$$

Here, E represents the energy position of the lower d-band edge for Eu^{2+} (cm^{-1}); Q (3400 cm^{-1} for Eu^{2+}) stands for the energy position for the low d-band edge of the free ion; V equals the valence of the cation (V = 2 for Eu^{2+}); n is the coordination number (CN) of the site occupied by activator ion; Ea is a constant in the same host; r is the radius of the cationic ion replaced by the activator. According to the CN of each cationic site, the radius of the five cationic sites decreased in the order of Ba2 (CN = 12, r = 1.61 Å) > K (CN = 10, r = 1.59 Å) > Ba1/Ba3 (CN = 9, r = 1.47 Å) > Ca (CN = 8, r = 1.12 Å). The Gaussian emission band peaked at 443, 500 and 535 nm was attributed to the emission of Eu^{2+} occupied the Ca, K and Ba2 sites, but it is impossible to distinguish the attribution of band centered at 460 and 481 from site Ba1 or Ba3 due to their same CN and radius. Fortunately, the crystal field strength is not only determined by the positive ionic radius and CN, but also by the type of the polyhedron and the bond length, *etc.* [30, 31]. Generally, the loose site means lower crystal field strength, which leads to smaller degree of crystal field splitting and higher-energy emission peak [32, 33]. For comparing the splitting degree strength of Eu^{2+} 5d orbits in sites Ba1 and Ba3, the bond length of Eu/Ba-O in two sites are listed in Table S1. Eu1(enter the sites of Ba1) is coordinated by 9 oxygen atoms with the average bond length 2.8236 Å, which is shorter than that of Eu3-O (2.8520 Å, at Ba3 site). Hence, the higher energy emission peak at 460 nm is probably originated from the 5d → 4f transitions of Eu^{2+} in Ba3 site, while the relative lower energy emission peak at 481 nm is ascribed to Eu^{2+} in Ba1 site.

3.3. Analysis of crystal field at Ba1 and Ba3.

In order to further identify the attribution of emission bands centered at 460 and 481 nm, the splitting of Eu^{2+} 5d orbits was determined through *first-principles computations*. First, the optimized structures of Eu^{2+} enter the Ba1 or Ba3 sites were established on the basis of the pristine BCKP structure, as shown in Figure 4a and b. It is found that the bond lengths of Eu1/3-O and Ba1/3-O in the optimized structure (in Table S3) is close to that of Rietveld refinement results,

which illuminates that the present optimized structures are reasonable. Based on this result, the PDOS on the *d* orbitals of Eu atom in Ba1 or Ba3 site were calculated using the *first-principles computations* (in Figure 4c and d), respectively.

As shown in the Figure 4c and d, the five PDOS spectra can be grouped into three groups in crystal field environment, including d_z^2, degenerate d_{xz} and d_{yz}, and the other degenerate d_{xy} and d_x^2-$_y^2$ orbitals. And each PDOS spectrum has split into two parts: one above the E_F and the other below it, which is the splitting between binding and anti-binding states of Eu-O bonds. *d*-orbital splitting is attributed to the spherical symmetry breaking under purterbation of surrounding O atoms, and the stronger purterbation corresponds to the larger splitting. Here the strength of purterbation shows positive correlation with the strength of Eu-O bonds, and the latter is related to the splitting between binding and anti-binding states of Eu-O bonds [34].

Comparing the splitting between binding and anti-binding states of the Eu1-O (in Ba1 site) and Eu3-O (in Ba3 site) bonds in different orbital groups, the splitting energy of Eu1 is obviously bigger (6.10 eV in d_z^2 orbital, 5.17 eV in d_{xz} and d_{yz} degenerate orbitals) than those of Eu3 (5.16 eV in d_z^2 orbital, 3.68 eV in d_{xz} and d_{yz} degenerate orbitals). These big differences derive from the shorter Eu1-O bond length than that of Eu3-O in vertical direction. And there are three O atoms around Eu1 but no O atoms around Eu3 in horizontal direction, which leads relatively weak interaction between degenerate orbitals d_x^2-$_y^2$, d_{xy} and surrounding O atoms for Eu3, thus the splitting energy of Eu^{2+} in degenerate orbitals d_x^2-$_y^2$ and d_{xy} is smaller for Eu3 (5.00 eV) in comparison with that of Eu1 (5.17 eV) in the PDOS spectra. Based on above mentioned, the splitting degree of Eu^{2+} 5d orbitals in Ba1 site is larger than that of Eu^{2+} 5d orbitals in Ba3 site, implying a stronger crystal field for Eu in Ba1 site. Therefore, the emission bands centered at 460 nm and 481 nm are attributed to the emission of Eu^{2+} in the sites of Ba3 and Ba1, respectively.

Above results accurately confirm that there are five Eu^{2+} luminescence centers, and the corresponding emission band centered at 443, 460, 481, 500 and 535 nm are from the Eu^{2+} occupied the sites of Ca, Ba3, Ba1, K and Ba2 in the host BCKP.

3.4. Thermal stability.

During the practical application of phosphor in LEDs, the working temperature of the LED chip would arrive at about 100 ℃. A perfect phosphor for LEDs should offer excellent thermal stability, which will be conductive to maintain high efficiency and long lifetime of the LEDs. As a result,

the temperature-dependent PL spectra of BCKP: 1%Eu^{2+} were showed in Figure 5a, in which the integrated intensity of sample continuously decreases with the temperature increase and remains at about 62% intensity at room temperature as heating up to 100 ^{o}C (Figure 5b). Generally, the emission intensity thermal quenching is attributed to non-radiative relaxation. With the temperature rising, more and more excited electrons absorb additional vibration energy to jump and arrive the cross point of ground and excited state, then the electrons return to the ground state in the form of releasing heat rather than light (inset of Figure 5b). The thermal quenching activation energy (E_a) can be figured out by the following formula: [35]

$$I_T = \frac{I_0}{1 + c\exp\left(-Ea/\kappa T\right)} \qquad (2)$$

Where I_T and I_0 represent emission intensities at experimental and room temperature, respectively; κ stands for the Boltzmann constant (κ = 8.617 × 10^{-5} eV/K); c (constant) is the rate of thermally activated escape. According to equation (2), the activated energy was calculated as E_a = 0.26 eV based on the slope of the straight line yielded by the plot of ln(I_0/I-1) *vs* 10000/T.

3.5. Enhancement of red component in Eu^{2+} doped BCKP.

The optimal composition of Eu^{2+} doped BCKP was determined according to the integrated intensities of PL spectra as function of Eu^{2+} concentration. As depicted in Figure S2, the intensity of samples first monotonously increase and arrive the maximum at 1% content. After that, the PL intensity rapidly decreases as the concentration of Eu^{2+} beyond 1% due to the concentration quenching effect, which is attributed to the non-radiative energy migration among the identical activator Eu^{2+} ions. From the PL spectra with different Eu^{2+} contents, it is found that the red component is deficient. However, the red light not only plays a super important role in photosynthetic apparatus development but also accelerates the accumulation of starch by inhabiting the translation of photosynthesis out of leaves [36, 37]; simultaneously, the red component is also benefit to obtain an ideal lighting source with improving CRI and CCT. Thus, it is necessary to enhance the weak red emission intensity for single-doped BCKP: Eu^{2+} in order to well meet the requirement of photosynthesis. It is an obvious approach through introduction Mn^{2+} in BCKP host because Mn^{2+} will has a orange to red emission in strong crystal field as it enters the sites of Ca in present new compound BCKP, in which efficient energy transfer (ET) from Eu^{2+} to Mn^{2+} is necessary. The PLE and PL spectra of Eu^{2+} and Mn^{2+} solely doped BCKP is showed in

Figure 6a and b, in which a significant spectral overlap was found between the PL spectrum of Eu^{2+}- and the PLE spectrum of Mn^{2+}-doped samples and the resonance-type energy transfer from Eu^{2+} to Mn^{2+} is possible occurred. After co-doping the Eu^{2+} and Mn^{2+} into the BCKP, the red component was greatly improved *(Figure S3)* and the PLE spectra of Eu^{2+} and Mn^{2+} co-doped BCKP phosphor are the similar under monitoring at 460 and 590 nm (Figure 6c), which further imply that the resonance-type energy transfer from Eu^{2+} to Mn^{2+} is existed. The decay curves of BCKP: 1%Eu^{2+}, *y*%Mn^{2+} were measured under the excitation of 375 nm and depicted in Figure 6d as a function of Mn^{2+} contents (*y*) to further confirm the occurrence of ET in the co-doped samples.

It is observed that the lifetime of Eu^{2+} gradually decline with the growth of Mn^{2+} concentration, and the decay curves can be well fitted with the second-order exponential decay model, as following equation: [38, 39]

$$I_t = I_0 + A_1 \exp\left(-\frac{t}{\tau_1}\right) + A_2 \exp\left(-\frac{t}{\tau_2}\right) \tag{3}$$

Here, I_0 and I_t are the luminescence intensity when times are 0 and *t*, respectively; A_1 and A_2 are fitting constants; τ_1 and τ_2 represent the fast and slow lifetimes for the exponential segment, respectively. According to the fitting results, the average lifetimes of Eu^{2+} monitored at 460 nm are calculated to be 501.79, 453.70, 412.27, 350.53, 273.64 ns with concentration of Mn^{2+} at y = 0, 5, 10, 15, 20, respectively. As the concentration of Mn^{2+} increasing, the average lifetimes decrease visibly, which further confirm the existence of ET from Eu^{2+} to Mn^{2+}. And the ET efficiency (η_τ) can be calculated by the equation: [40]

$$\eta_\tau = 1 - \frac{\tau}{\tau_0} \tag{4}$$

Where τ_0 and τ stand for the decay lifetimes of the sensitizer in singly and co-doped samples. The dependence of τ and η_τ on the Mn^{2+} concentration is displayed in inset of Figure 5b, where the ET efficiency rise from 0 to 45.5% with the contents of the Mn^{2+} increasing from 0 to 20%. And the ET process can be described as: the electrons of Eu^{2+} are pumped to excited state 5d from ground state 4f with the excitation of 365 nm n-UV light, and then non-radiatively (NR) back to the lowest excited level. Afterwards part of them back to the ground state with a cyan emission while the other part of energy transfer to Mn^{2+} resulting in the excitation of the electrons from ground

state to excited state, leading to the enhanced red emission by the ET process from Eu^{2+} to Mn^{2+} ions. Meanwhile, the ET mechanism has also been investigated on the base of the Dexter's ET expression of exchange interaction and multi-polar interaction by the following relation: [41, 42]

$$\frac{\eta_0}{\eta} \propto C^{\frac{\theta}{3}}, \quad \frac{I_0}{I} \propto C^{\frac{\theta}{3}} \tag{5}$$

Here, η_0 and η represent the luminescence quantum efficiency of Eu^{2+} ions with or without Mn^{2+} ions; C stands for the dope contents of Mn^{2+}; the value of η_0/η can be approximately estimated by the ratio of related luminescence intensities (I_0/I); θ = 3, 6, 8, and 10 corresponded to exchange interaction, dipole-dipole, dipole-quadrupole and quadrupole-quadrupole interaction, respectively. The most reasonable linear relation was observed when θ = 6 in the I_0/I *vs* $C^{\theta/3}$ plots, which imply the dipole-dipole mechanism dominates the $ET_{Eu\text{-}Mn}$ in the BCKP host (Figure S4).

3.6. Fabrication and performance of the white LED.

To evaluate the practical application of the synthesized phosphors, two devices were fabricated by combining 365 nm LED chips with Eu^{2+} solely (LED 1) and Eu^{2+}/Mn^{2+} co-doped (LED 2) BCKP, respectively. Comparing properties of LED1 and LED2, it is obviously observed that the device parameters of LED2 are better than those of LED1, which indicates that the introduction of Mn^{2+} in the phosphor effectively improve the property of LED devices due to the enhancement of red component in the spectrum. Figure 7b displays the emission spectrum of LED 2 together with the absorption spectra of the carotenoid and chlorophyll-b, and an obvious overlap was found between them. Results further indicate that the present sample BCKP: 1%Eu^{2+}, 20%Mn^{2+} not only can be effectively excite by n-UV LED chip to emit warm white light, but also can be used to promote the plant growth. In comparing traditional red and blue double band LEDs, the LEDs fabricated with present Eu^{2+}-Mn^{2+} co-doped BCKP phosphor are more appropriate for plant growth and offer more comfortable light environment for the operator.

4. Conclusions

In summary, a new family of compounds with representative compound $Ba_3CaK(PO_4)_3$ (BCKP) was synthesized *via* high-temperature solid-state reaction method, its structure was solved in direct space and refined by Rietveld method. Crystal structure possesses five cationic sites

including $Ba1O_9$, $Ba2O_{12}$, $Ba3O_9$, CaO_8 and KO_{10} on the base of the XRD Rietveld refinements. The phosphor BCKP: 1%Eu^{2+} emits a bright cold white light with about 90% QE and including five luminescent centers. Its complicated multi-luminescence centers were clearly assigned by low temperature spectra (LHT), TRES and the Van Uitert equation. The *first-principles calculations* was used to compute the *d*-orbital splitting energy to distinguish the assignment of peaks at 460 and 482 nm since Eu^{2+} at Ba1 or Ba3 sites has same CN and ionic radius. The emission centers of Eu^{2+} in crystallographic sites Ca, Ba1, Ba3, K and Ba2 are corresponded to the Gaussian fitting peaks at 430, 460, 481, 550 and 535 nm in BCKP: 1%Eu^{2+}, respectively. Additionally, the red component has been enhanced by introducing Mn^{2+} into BCKP: 1%Eu^{2+} and the QE of the co-doped sample remains 65%, and the ET process from Eu^{2+} to Mn^{2+} ions has been investigated in detail by photoluminescence spectra and decay curves. White LED devices were also fabricated by combining co-doped sample with 365 nm chip, which not only exhibits a excellent Ra (92) and CCT (4486 K) but also its spectra coincides well with the absorption spectra of the carotenoid and chlorophyll-b. Results indicate that the phosphor BCKP: Eu^{2+}, Mn^{2+} has great potential application in white LEDs and plant growth supplement lighting source.

Acknowledgments

This work was supported by National Natural Science Foundation of China (No. 11704312, 51672215, 11274251), Research Fund for the Doctoral Program of Higher Education of China (RFDP) (No.20136101110017) and by RFBR (17-52-53031).

Appendix A. Supplementary data

Supplementary data associated with this article can be found, in the online version.

References

[1] A. Agarwal, S. D. Gupta, Impact of light-emitting diodes (LEDs) and its potential on plant growth and development in controlled-environment plant production system, Curr. Biotechnol. 5 (2016) 28-43.

[2] M. Olle, A. Viršilė, The Effects of light-emitting diode lighting on greenhouse plant growth

and quality, Agric. food Sci. 22 (2013) 223-234.

[3] G. Tamulaitis, P. Duchovskis, Z. Bliznikas, K. Breivel, R. Ulinskaite, A. Brazaityte, A. Novikovas, A. Zukauskas, High-power light-emitting diode based facility for plant cultivation, J. Phys. D: Appl. Phys. 38 (2005) 3182-3187.

[4] A. Shimada, Y. Taniguchi, Red and blue pulse timing control for pulse width modulation light dimming of light emitting diodes for plant cultivation, J. Photoch. Photobio. B 104 (2011) 399–404.

[5] J. Y. Chen, N. M. Zhang, C. F. Guo, F. J. Pan, X. J. Zhou, H. Suo, X. Q. Zhao, E. M. Goldys, Site-dependent luminescence and thermal stability of Eu^{2+} doped fluorophosphate toward white LEDs for plant growth, ACS Appl. Mater. Interfaces 8 (2016) 20856-20864.

[6] Z. W. Zhou, J. M. Zheng, R. Shi, N. M. Zhang, J. Y. Chen, R. Y. Zhang, H. Suo, E. M. Goldys, C. F. Guo, Ab initio site occupancy and far-red emission of Mn^{4+} in cubic-phase $La(MgTi)_{1/2}O_3$ for plant cultivation, ACS Appl. Mater. Interfaces 9 (2016) 6177-6185.

[7] R. S. Liu, Phosphors, Up conversion nano particles, quantum dots and their applications, in: C. F. Guo, H. Suo (Eds.), Design of Single-phased Multicolor-emission Phosphor for LED, Springer Berlin, Heidelberg, 2017, pp. 459-508.

[8] L. Ma, D. J. Wang, Z. Y. Mao, Q. F. Lu, Z. H. Yuan, Investigation of Eu–Mn energy transfer in $A_3MgSi_2O_8$: Eu^{2+}, Mn^{2+} (A = Ca, Sr, Ba) for light-emitting diodes for plant cultivation, Appl. Phys. Lett. 93 (2008) 144101.

[9] C. F. Guo, X. Ding, L. Luan, Y. Xu, Two-color emitting of Eu^{2+} and Mn^{2+} co-doped $Sr_2Mg_3P_4O_{15}$ for UV LEDs, Sensor. Actuat. B 143 (2010) 712-715.

[10] A. Stockman, D. I. A. MacLeod, N. E. Johnson, Spectral sensitivities of the human cones, J. Opt. Soc. Am. A 10 (1993) 2491-2521.

[11] G. D. Massa, H. H. Kim, R. M. Wheeler, C. A. Mitchell, Plant productivity in response to LED lighting, HortScience 43 (2008) 1951-1956.

[12] Y. Sato, H. Kato, M. Kobayashi, T. Masaki, D. H. Yoon, M. Kakihana, Tailoring of deep-red luminescence in Ca_2SiO_4: Eu^{2+}, Angew. Chem., Int. Ed. 53 (2014) 7756-7759.

[13] H. P. Ji, Z. H. Huang, Z. G. Xia, M. S. Molokeev, V. V. Atuchin, M. H. Fang, Y. G. Liu, Discovery of new solid solution phosphors via cation substitution-dependent phase transition in $M_3(PO_4)_2$:Eu^{2+} (M = Ca/Sr/Ba) quasi-binary sets, J. Phys. Chem. C 119 (2015) 2038-2054.

[14] M. Y. Chen, Z. G. Xia, M. S. Molokeev, C. C. Lin, C. C. Su, Y. C. Chuang, Q. L. Liu, Probing Eu^{2+} luminescence from different crystallographic sites in $Ca_{10}M(PO_4)_7:Eu^{2+}$ (M = Li, Na, and K) with β-$Ca_3(PO_4)_2$-type structure, Chem. Mater. 29 (2017) 7563-7570.

[15] C. H. Huang, Y. C. Chiu, Y. T. Yeh, T. S. Chan, T. M. Chen, Eu^{2+}-activated $Sr_8ZnSc(PO_4)_7$: a novel near-ultraviolet converting yellow-emitting phosphor for white light-emitting diodes, ACS appl. Mater. Interfaces 4 (2012) 6661-6668.

[16] Bruker, A. TOPAS, V4: General profile and structure analysis software for powder diffraction data; User's Manual; Bruker AXS: Karlsruhe, Germany, 2008.

[17] J. P. Perdew, K. Burke, M. Ernzerhof, Generalized gradient appromximate made simple, Phys. Rev. Lett. 77 (1996) 3865-3868.

[18] H. J. Monkhorst, J. D. Pack, Special points for brillouin-zone integrations, Phys. Rev. B 13 (1976) 5188-5192.

[19] *PLATON*–A multipurpose crystallographic tool; Utrecht University, Utrecht, The Netherlands, 2008.

[20] R. D. Shannon, Revised effective ionic radii and systematic studies of interatomic distances in halides and chalcogenides, Acta Crystallogr. A 32 (1976) 751-767.

[21] T. Naddari, H. El Feki, J. M. Savariault, Structure and ionic conductivity of the lacunary apatite $Pb_6Ca_2Na_2(PO_4)_6$, Solid State Ionics 158 (2003) 157-166.

[22] A. A. Belik, L. N. Ivanov, B. I. Lazoryak, V. B. Gutan, Synthesis, structure, and luminescence properties of $Ca_9MnM(PO_4)_7$ (M = Li, Na, K), Zhurnal Neorganicheskoj Khimii 46 (2001) 885-892.

[23] T. J. McCoy, I. M. Steele, K. Keil, B. F. Leonard, M. Endre, Chladniite, $Na_2CaMg_7(PO_4)_6$: a new mineral from the carleton (IIICD) iron meteroite, Am. Mineral. 79 (1994) 375-380.

[24] M. Kim, M. Kobayashi, H. Kato, H. Yamane, Y. Sato, M. Kakihana, Crystal structures and luminescence properties of Eu^{2+}-activated new $NaBa_{0.5}Ca_{0.5}PO_4$ and $Na_3Ba_2Ca(PO_4)_3$, Dalton Trans. 44 (2015) 1900-1904.

[25] Y. Yonesaki, C. Matsuda, Q. Dong, Structural consideration on the emission properties of Eu^{2+}-doped $Li_2BaMgP_2O_8$ and $Na_2BaMgP_2O_8$ orthophosphates, J. Solid State Chem. 196 (2012) 404-408.

[26] A. Boukhris, M. Hidouri, B. Glorieux, M. B. Amara, $Na_2BaMg(PO_4)_2$: synthesis, crystal

structure and europium photoluminescence properties, J. Rare Earth. 31 (2013) 849-856.

[27] K. Geng, Z. G. Xia, M. S. Molokeev, Crystal structure and luminescence property of a novel blue-emitting $Cs_{2x}Ca_{2x}Gd_{2(1-x)}(PO_4)_2$: Eu^{2+} (x = 0.36) phosphor, Dalton Trans. 43 (2014) 14092-14098.

[28] W. Z. Lv, Y. C. Jia, Q. Zhao, W. Lu, M. M. Jiao, B. Q. Shao, H. P. You, Synthesis, structure, and luminescence properties of $K_2Ba_7Si_{16}O_{40}$:Eu^{2+} for white light emitting diodes, J. Phys. Chem. C 118 (2014) 4649-4655.

[29] W. Z. Sun, Y. L. Jia, R. Pang, H. F. Li, T. F. Ma, D. Li, J. P. Fu, S. Zhang, L. H. Jiang, C. Y. Li, $Sr_9Mg_{1.5}(PO_4)_7$: Eu^{2+}: a novel broadband orange-yellow-emitting phosphor for blue light-excited warm white LEDs, ACS Appl. Mater. Interfaces 7 (2015) 25219-25226.

[30] A. L. Companion, M. A. Komarynsky, Crystal field splitting diagrams, J. Chem. Educ. 41 (1964) 257-262.

[31] P. A. Tanner, L. X. Ning, Electronegativity, charge transfer, crystal field strength, and the point charge model revisited, J. Phys. Chem. A 117 (2013) 1503-1507.

[32] K. S. Sohn, S. J. Lee, R. J. Xie, N. Hirosaki, Time-resolved photoluminescence analysis of two-peak emission behavior in $Sr_2Si_5N_8$: Eu^{2+}, Appl. Phys. Lett. 95 (2009) 121903.

[33] C. Grieco, K. F. Hirsekorn, A. T. Heitsch, A. C. Thomas, M. H. McAdon, B. A. Vanchura, M. M. Romanelli, L. L. Brehm, A. Leugers, A. Sokolov, J. B. Asbury, Mechanisms of energy transfer and enhanced stability of carbidonitride phosphors for solid state lighting, ACS Appl. Mater. Interfaces 9 (2017) 12547-12555.

[34] J. Stöhr, H. C. Siegmann, Magnetism: from fundamentals to nanoscale dynamics, Springer Science & Business Media, 2007.

[35] X. J. Zhang, J. Wang, L. Huang, F. J. Pan, Y. Chen, B. F. Lei, M. Y. Peng, M. M. Wu, Tunable luminescence properties and concentration-dependent, site-preferable distribution of Eu^{2+} ions in silicate glass for white LEDs applications, ACS Appl. Mater. Interfaces 7 (2015) 10044-10054.

[36] D. L. Dexter, J. H. Schulman, Theory of concentration quenching in inorganic phosphors, J. Chem. Phys. 22 (1954) 1063-1070.

[37] M. C. Wu, C. Y. Hou, C. M. Jiang, Y. T. Wang, C. Y. Wang, H. H. Chen, H. M. Chang, A novel approach of LED light radiation improves the antioxidant activity of pea seedlings, Food Chem. 101 (2007) 1753–1758.

[38] H. Suo, C. F. Guo, Z. Yang, S. S. Zhou, C. K. Duanb, M. Yin, Thermometric and optical heating Bi-functional properties of upconversion phosphor $Ba_5Gd_8Zn_4O_{21}$:Yb^{3+}/Tm^{3+}, J. Mater. Chem. C 3 (2015) 7379-7385.

[39] K. Li, J. Fan, M. M. Shang, H. Z. Lian, J. Lin, $Sr_2Y_8(SiO_4)_6O_2$: Bi^{3+}/Eu^{3+}: a single-component white-emitting phosphor via energy transfer for UVw-LEDs, J. Mater. Chem. C 3 (2015) 9989-9998.

[40] J. Chen, Y. G. Liu, M. H. Fang, Z. H. Huang, Luminescence properties and energy transfer of Eu/Mn-coactivated $Mg_2Al_4Si_5O_{18}$ as a potential phosphor for white-light LEDs, Inorg. Chem. 53 (2014) 11396-11403.

[41] Y. J. Zheng, H. M. Zhang, H. R. Zhang, Z. G. Xia, Y. L. Liu, M. S. Molokeev, B. F. Lei, Co-substitution in $Ca_{1-x}Y_xAl_{12-x}Mg_xO_{19}$ phosphors: Local structure evolution, photoluminescence tuning and application for plant growth LEDs, J. Mater. Chem. C 6 (2018) 4217-4224.

[42] Y. W. Zhu, L. Y. Cao, M. G. Brik, x. J. Zhang, L. Huang, T. T. Xuan, J. Wang, Facile synthesis, morphology and photoluminescence of a novel red fluoride nanophosphor K_2NaAlF_6: Mn^{4+}, J. Mater. Chem. C 5 (2017) 6420-6426.

Figure and Table captions

Figure 1. Rietveld refinement XRD patterns of blank BCKP (a) as well as BCKP: 1%Eu^{2+}, 20%Mn^{2+} (b) together with crystal structure of the BCKP host and cationic sites (c).

Figure 2. The PL and PLE spectra (a) and the normalized two-dimensional time-resolved emission spectra (TRES) (b) together with the normalized spectra slices of TRES at 1.0, 1.5, 2.5, 4.5 μs (c) of the 1%Eu^{2+} doped BCKP at room temperature.

Figure 3. The PL spectrum of BCKP: Eu^{2+} at liquid helium temperature with the Gaussian fitting peaks and five cationic sites.

Figure 4. The optimized structure of BCKP and the projector density of states (PDOS) of the *d*-orbital splitting energy level of Eu^{2+} doped into Ba1 (a, c) or Ba3 (b, d) site.

Figure 5. (a) Temperature-dependent two-dimensional photoluminescence spectrum (λ_{ex} = 365 nm), (b) integrated PL intensity and (c) activation energy of thermal quenching of BCKP: 1%Eu^{2+}. The inset shows the schematic configuration coordinate diagram of the Eu^{2+} ion.

Figure 6. (a) PLE and PL spectra of (a) 1%Eu^{2+}, (b) 10%Mn^{2+} and (c) 1%Eu^{2+}, 20%Mn^{2+} doped BCKP; (d) the decay time of BCKP: 1%Eu^{2+}, *y*%Mn^{2+} (*y* = 0, 5, 10, 15, 20) and the inset shows ET efficiency from Eu^{2+} to Mn^{2+} with different contents of Mn^{2+}.

Figure 7. The chromaticity coordinates of two white LED devices fabricated by combining 365 nm chips with phosphors BCKP: 1%Eu^{2+} (No.1) and BCKP: 1%Eu^{2+}, 20%Mn^{2+} (No.2) (a) together with the emission spectra of No.2 white LED device along with the absorption spectra of carotenoid and chlorophyll-b (b).

Table 1. Rietveld refinement and crystallographic parameters of BCKP and BCKP: 1%Eu^{2+}, 20%Mn^{2+}.

Figures and Table

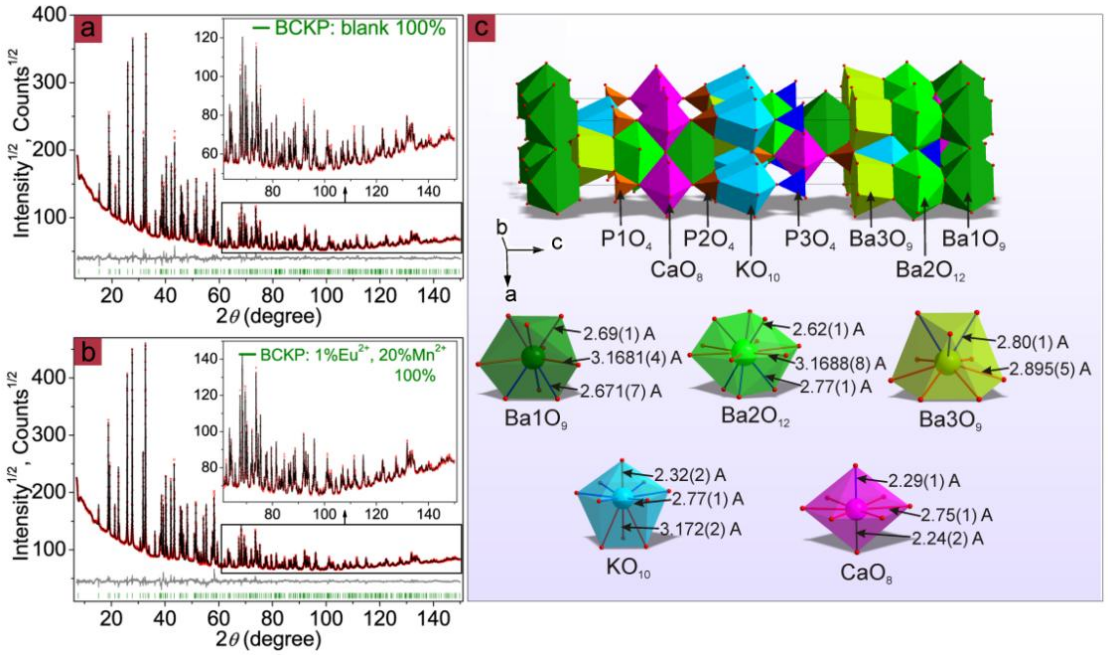

Figure 1. Rietveld refinement XRD patterns of blank BCKP (a) as well as BCKP: 1%Eu^{2+}, 20%Mn^{2+} (b) together with crystal structure of the BCKP host and cationic sites (c).

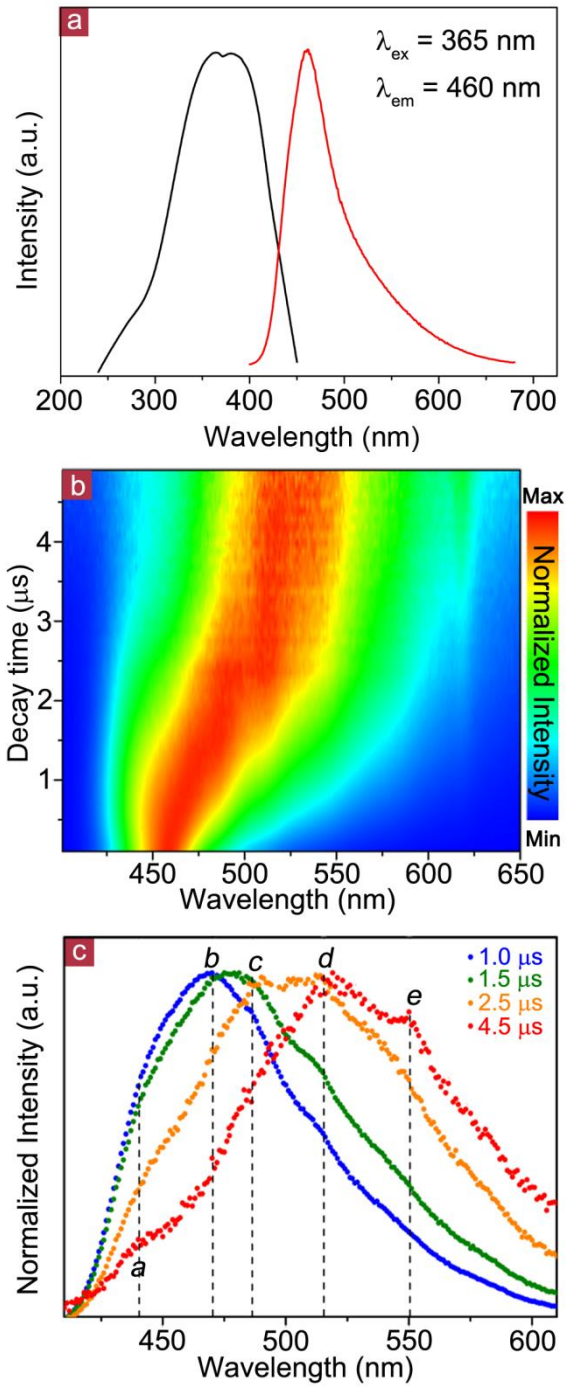

Figure 2. The PL and PLE spectra (a) and the normalized two-dimensional time-resolved emission spectra (TRES) (b) together with the normalized spectra slices of TRES at 1.0, 1.5, 2.5, 4.5 μs (c) of the 1%Eu^{2+} doped BCKP at room temperature.

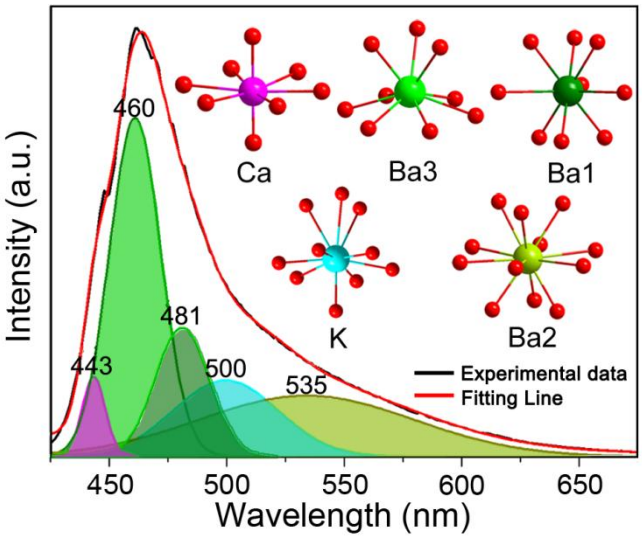

Figure 3. The PL spectrum of BCKP: Eu^{2+} at liquid helium temperature with the Gaussian fitting peaks and five cationic sites.

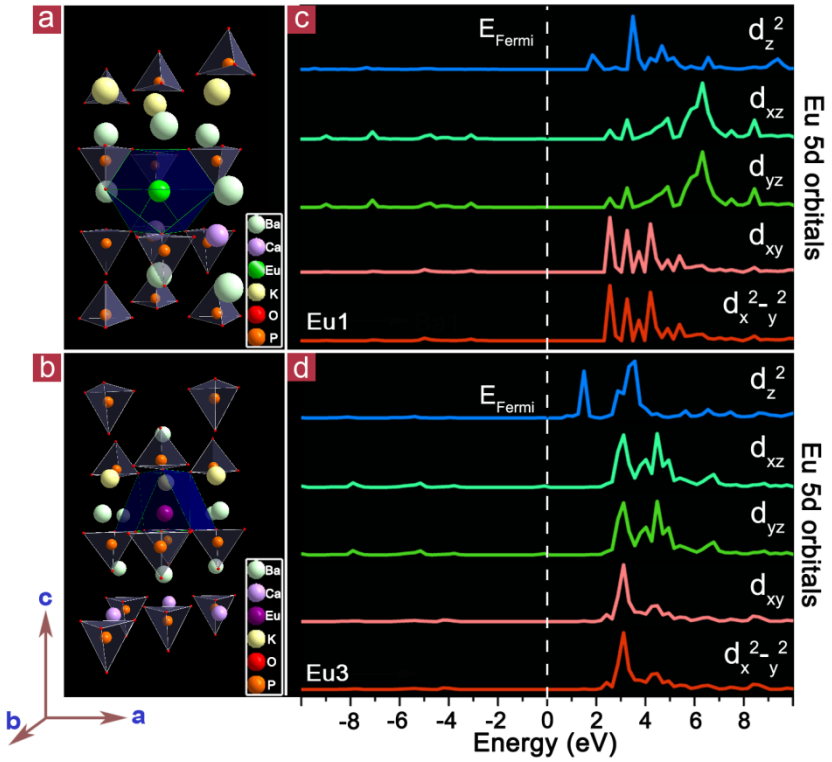

Figure 4. The optimized structure of BCKP and the projector density of states (PDOS) of the *d*-orbital splitting energy level of Eu^{2+} doped into Ba1 (a, c) or Ba3 (b, d) site.

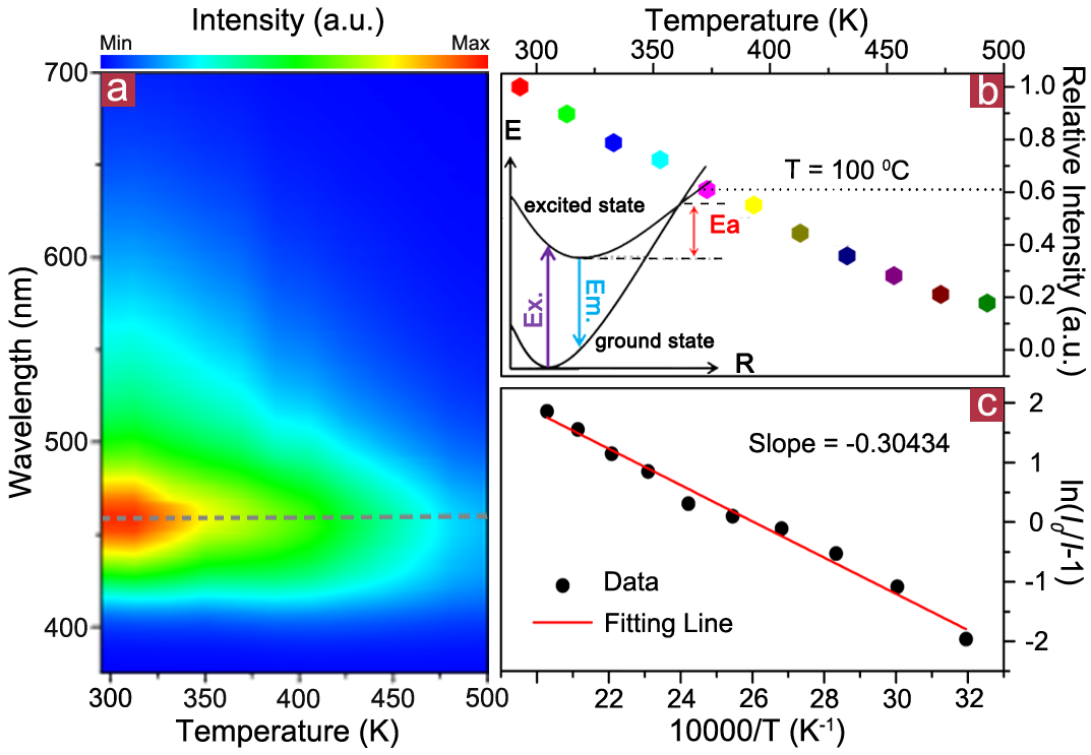

Figure 5. (a) Temperature-dependent two-dimensional photoluminescence spectrum (λ_{ex} = 365 nm), (b) integrated PL intensity and (c) activation energy of thermal quenching of BCKP: 1%Eu^{2+}. The inset shows the schematic configuration coordinate diagram of the Eu^{2+} ion.

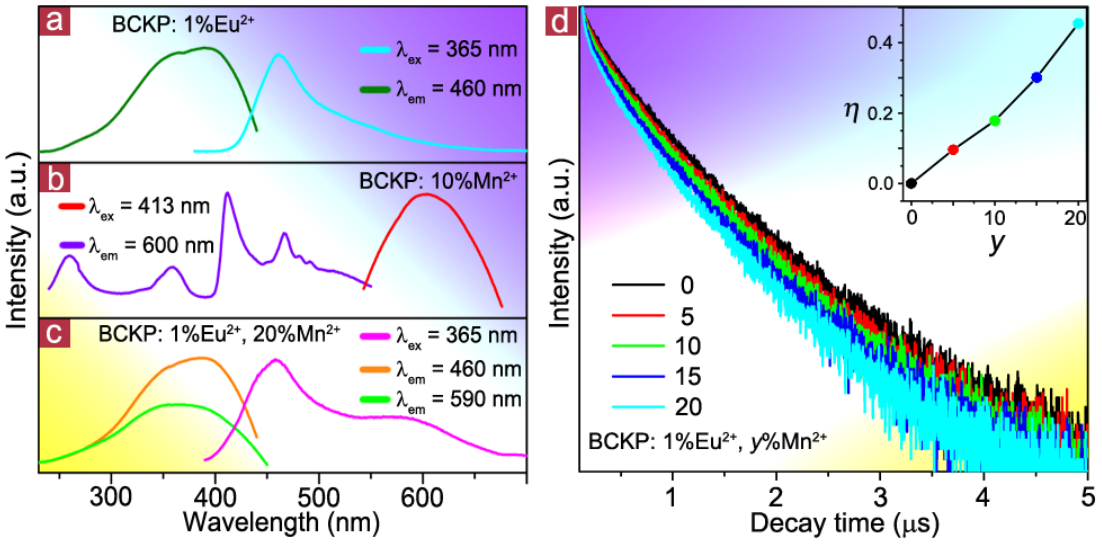

Figure 6. (a) PLE and PL spectra of (a) 1%Eu^{2+}, (b) 10%Mn^{2+} and (c) 1%Eu^{2+}, 20%Mn^{2+} doped BCKP; (d) the decay time of BCKP: 1%Eu^{2+}, *y*%Mn^{2+} (*y* = 0, 5, 10, 15, 20) and the inset shows ET efficiency from Eu^{2+} to Mn^{2+} with different contents of Mn^{2+}.

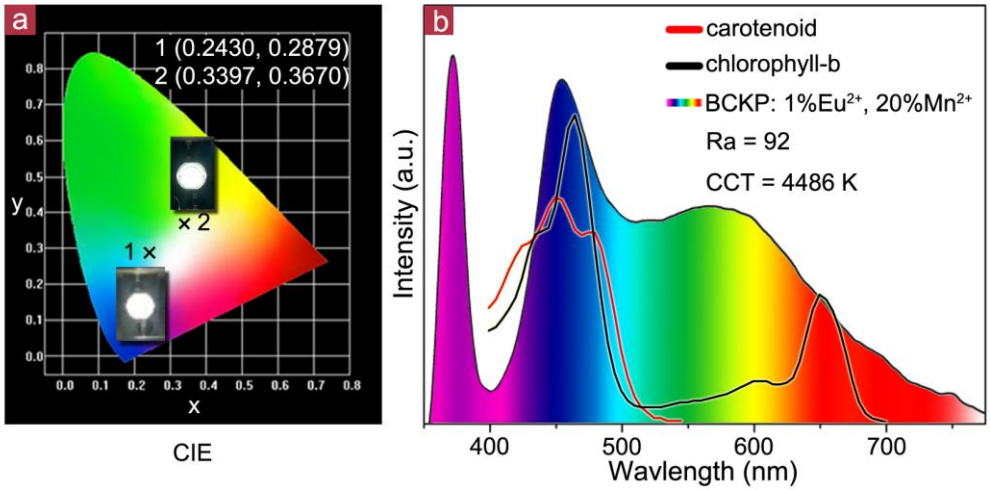

Figure 7. The chromaticity coordinates of two white LED devices fabricated by combining 365 nm chips with phosphors BCKP: 1%Eu^{2+} (No.1) and BCKP: 1%Eu^{2+}, 20%Mn^{2+} (No.2) (a) together with the emission spectra of No.2 white LED device along with the absorption spectra of carotenoid and chlorophyll-b (b).

Table 1. Rietveld refinement and crystallographic parameters of BCKP and BCKP: 1%Eu^{2+}, 20%Mn^{2+}.

Compound	**BCKP**	**BCKP: 1%Eu^{2+}, 20%Mn^{2+}**
space group	*R*3*m*	*R*3*m*
***a*, Å**	5.48501 (8)	5.48114 (3)
***c*, Å**	34.9204 (5)	34.9175 (2)
***V*, Å^3**	909.84 (3)	908.48 (1)
Z	3	3
***2θ*-interval, °**	7-150	7-150
R_{wp}, %	3.46	3.26
R_p, %	2.75	2.61
R_{exp}, %	0.94	0.76
χ^2	3.68	4.29
R_B, %	2.94	2.55

Graphical abstract

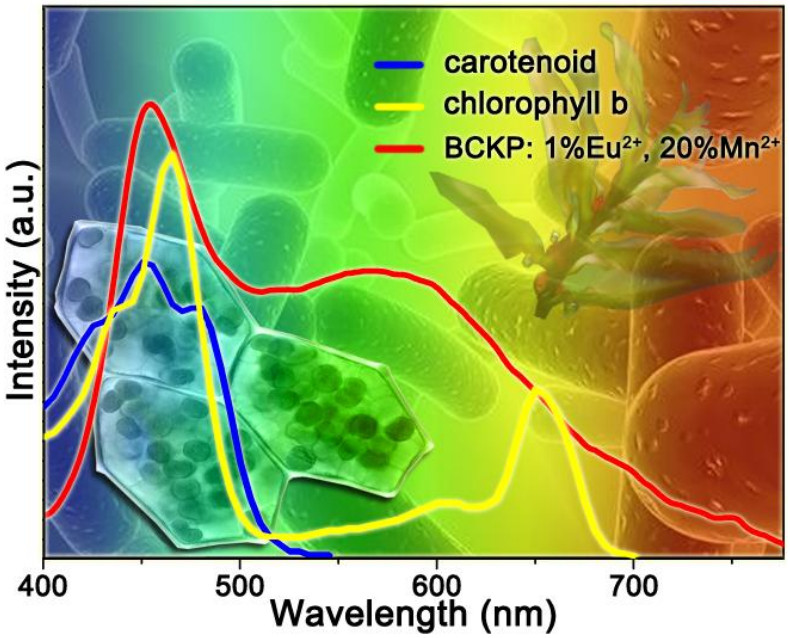

Supplementary Material

Click here to download Supplementary Material: 15-supported information.docx